Article

Current Biology

Chromosome choreography during the non-binary cell cycle of a predatory bacterium

Graphical abstract

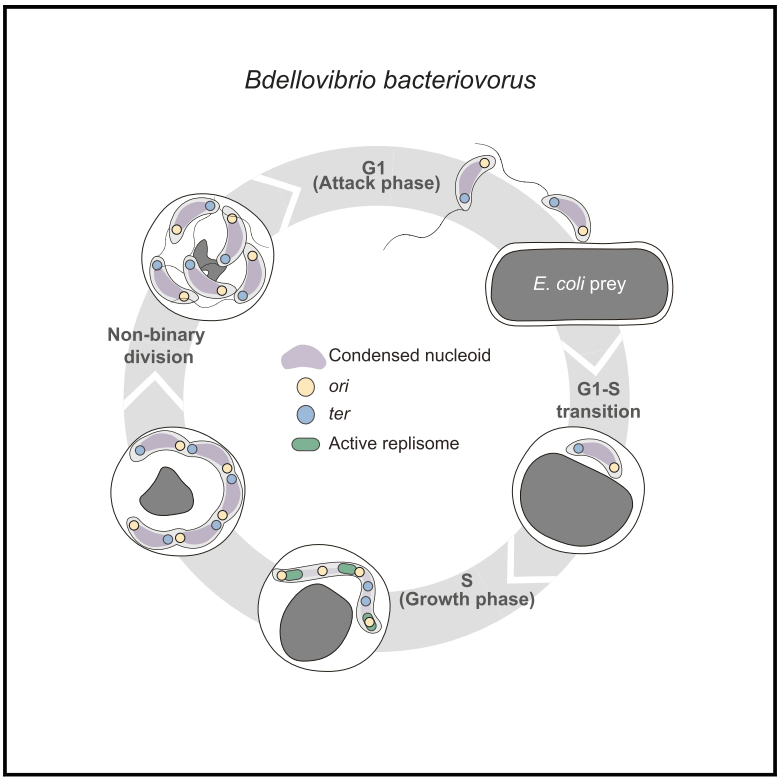

Authors

Jovana Kaljević, Terrens N.V. Saaki, Sander K. Govers, Ophélie Remy, Renske van Raaphorst, Thomas Lamot, Géraldine Laloux

Correspondence

geraldine.laloux@uclouvain.be

In brief

Kaljević et al. study non-binary proliferation in the predatory bacterium *Bdellovibrio bacteriovorus*. Examination of the spatiotemporal dynamics of its DNA throughout the cell cycle reveals that, as the predator elongates, concomitant rounds of replication and segregation generate chromosome copies for more than two daughter cells.

Highlights

- The *Bdellovibrio* chromosome is polarized, with *ori* located near the invasive pole
- The highly compacted nucleoid excludes cytosolic proteins in non-replicative cells
- Replication and segregation of chromosomes are uncoupled from cell division
- The centromeric protein ParB localizes at *parS* in a cell-cycle-dependent manner

Kaljević et al., 2021, Current Biology *31*, 3707–3720
September 13, 2021
https://doi.org/10.1016/j.cub.2021.06.024

CellPress

Current Biology

CellPress
OPEN ACCESS

Article

Chromosome choreography during the non-binary cell cycle of a predatory bacterium

Jovana Kaljević,[1] Terrens N.V. Saaki,[1] Sander K. Govers,[1,2] Ophélie Remy,[1] Renske van Raaphorst,[1] Thomas Lamot,[1] and Géraldine Laloux[1,3,4,*]

[1]de Duve Institute, UCLouvain, 75 Avenue Hippocrate, 1200 Brussels, Belgium
[2]Howard Hughes Medical Institute, Stanford University, Stanford, CA 94305, USA
[3]Twitter: @LalouxLab
[4]Lead contact
*Correspondence: geraldine.laloux@uclouvain.be
https://doi.org/10.1016/j.cub.2021.06.024

SUMMARY

In bacteria, the dynamics of chromosome replication and segregation are tightly coordinated with cell-cycle progression and largely rely on specific spatiotemporal arrangement of the chromosome. Whereas these key processes are mostly investigated in species that divide by binary fission, they remain mysterious in bacteria producing larger number of descendants. Here, we establish the predatory bacterium *Bdellovibrio bacteriovorus* as a model to investigate the non-binary processing of a circular chromosome. We found that its single chromosome is highly compacted in a polarized nucleoid that excludes freely diffusing proteins during the non-proliferative stage of the cell cycle. A binary-like cycle of DNA replication and asymmetric segregation is followed by multiple asynchronous rounds of replication and progressive ParABS-dependent partitioning, uncoupled from cell division. Finally, we provide the first evidence for an on-off behavior of the ParB protein, which localizes at the centromere in a cell-cycle-regulated manner. Altogether, our findings support a model of complex chromosome choreography leading to the generation of variable, odd, or even numbers of offspring and highlight the adaptation of conserved mechanisms to achieve non-binary reproduction.

INTRODUCTION

Bacteria thrive in highly diverse environments to which they finely adapt, as illustrated by the immense variety of proliferation modes that were selected through evolution. Despite this tremendous diversity, most of our knowledge about bacterial multiplication derives from work on a subset of model species, which all divide by binary fission: one mother cell elongates, duplicates its genetic information, and gives rise to two daughter cells upon a single cell division event.[1] However, not all bacteria adhere to the simple paradigm of binary reproduction.[2] Species from various lineages (including Actinobacteria, Cyanobacteria, and Bdellovibrionata) rely on sophisticated cell cycles involving multiple fission.[3–5] Here, larger and sometimes variable numbers of progeny are generated from a polyploid mother cell, through several (sequential or synchronous) septation events. The non-binary proliferation of these species, which is inherently complex due to the production of more than two descendants, offers an attractive platform to shed light on overlooked cell-cycle regulation strategies in bacteria.

To achieve each cell cycle with precision, bacterial cells rely on specific and elaborate spatiotemporal organization. A prominent example of cellular organization in bacteria is the intricate coordination, in both space and time, of chromosome replication and segregation with other cell-cycle events, including growth and cell division.[6] In model bacteria, the spatial and temporal organization of the chromosome depends on specific subcellular positions of key chromosomal loci, mainly the replication origin (*ori*) and terminus (*ter*), which display highly regulated dynamics during the cell cycle.[7–18] Soon after replication initiation, most species studied so far (with the exception of γ-proteobacteria) employ the ParABS system to actively partition sister *ori*.[19] In this system, directionality of *ori* segregation is provided by the exquisite interplay between the ParB protein, which binds and spreads from the centromeric *parS* sites near *ori*, and the unspecific DNA-binding ATPase ParA. Iterations of ParB-triggered ATPase activity and dissociation of ParA from the chromosome result in the segregation of duplicated ParB·*parS* complexes, before the replication forks reach the chromosomal *ter*.[20,21] Specific mechanisms physically connect the partitioning of *ter* copies with cell constriction, thereby coordinating the last steps of chromosome segregation and cell division[22–24] and ensuring that each daughter cell is equipped with a full set of genetic material. Except in some Streptomycetes,[25,26] the spatiotemporal organization of the chromosome and the interplay between fundamental cellular processes remain essentially unexplored in non-binary growing bacteria.

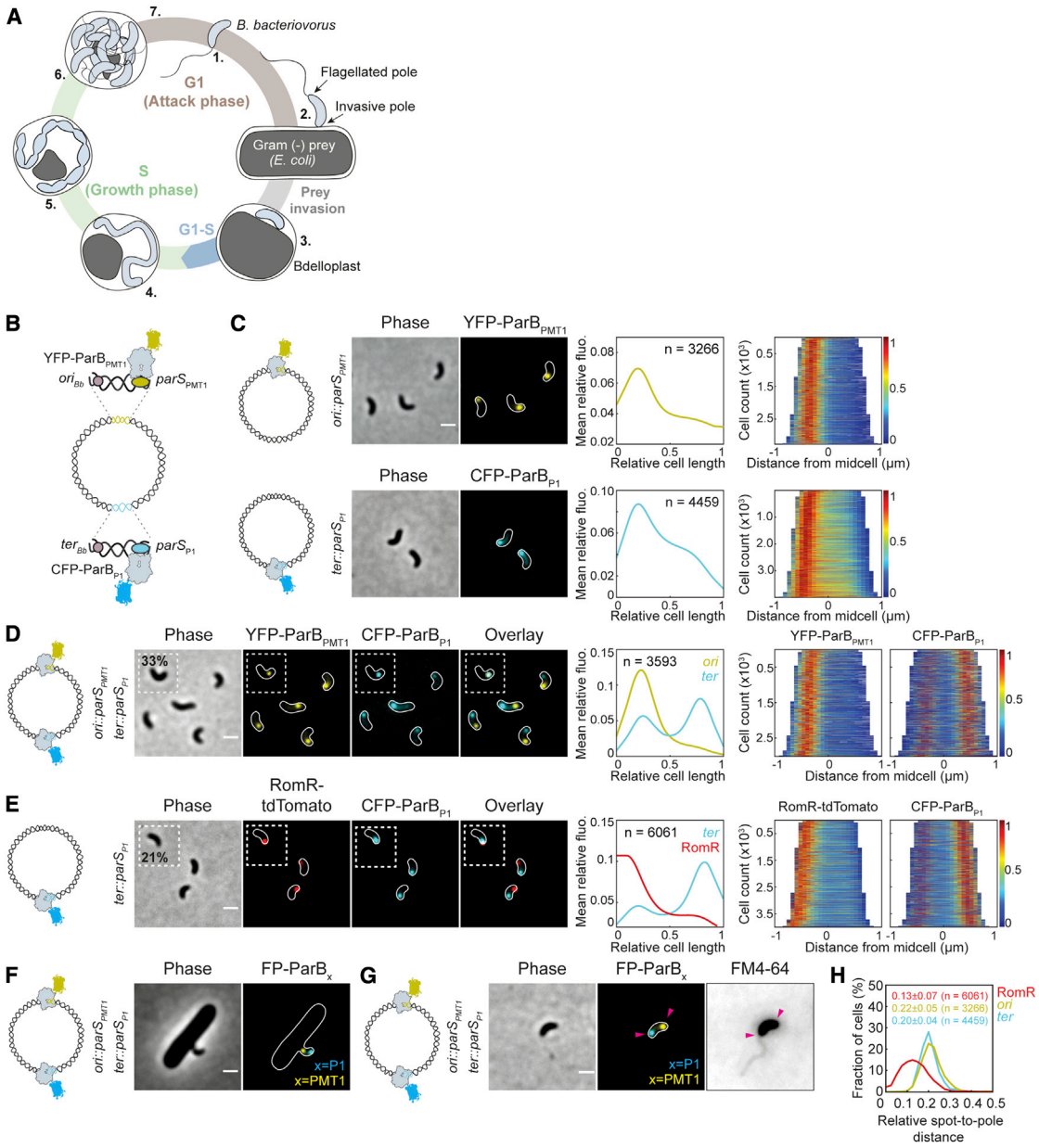

Figure 1. Linear arrangement of the *B. bacteriovorus* chromosome and localization of *ori* near the invasive pole

(A) Schematics of the *Bdellovibrio bacteriovorus* cell cycle. Numbers indicate key steps in the cycle: 1. Freely swimming attack phase (AP) cells. 2. Attachment of *B. bacteriovorus* to its prey, via pili located at the non-flagellated (invasive) pole. 3. *B. bacteriovorus* resides in the periplasm of the prey, which is now called bdelloplast. 4. Filamentous growth and consumption of prey content. 5. Pre-divisional state. 6. Non-binary division of the mother cell generates an odd or even number of daughter cells, which mature before 7. escaping the prey remnants and resuming the cell cycle. Attack phase (AP) and growth phase (GP) represent the G1 (non-replicative) and S (replicative) stages of the cell cycle, respectively. A G1-S transition takes place upon prey invasion (see Results).

(B) Schematics of the orthologous *parS*-ParB pairs used in this study to label chromosomal loci. The $parS_{PMT1}$/$parS_{P1}$ sequences (yellow/cyan) were integrated near the origin of replication (ori_{Bb}) or terminus of replication (ter_{Bb}) and the cognate YFP-ParB$_{PMT1}$ or CFP-ParB$_{P1}$ fluorescent fusions were constitutively produced from a replicative plasmid, respectively. Strains carrying $parS_{PMT1}$ or $parS_{P1}$ are respectively referred to as *ori*::$parS_{PMT1}$ or *ter*::$parS_{P1}$. Loci where $parS_{PMT1}$ or $parS_{P1}$ were integrated are respectively referred to as *ori* or *ter*.

(C) *ori* and *ter* are polarly localized. Left to right: representative phase contrast and fluorescence images of AP cells of *ori*::$parS_{PMT1}$ and *ter*::$parS_{P1}$ strains expressing cognate YFP-ParB$_{PMT1}$ and CFP-ParB$_{P1}$ (GL868 and GL771, respectively); mean pole-to-pole profiles of relative fluorescence intensity of the corresponding fusion in the same cells; demographs of the corresponding fluorescent signal in the same cells sorted by length and oriented based on signal intensity. Heatmaps represent relative fluorescence intensities.

(D) *ori* and *ter* occupy opposite poles in most cells. Left to right: representative phase contrast and fluorescence images of AP cells of a *ori*::$parS_{PMT1}$ *ter*::$parS_{P1}$ strain expressing cognate CFP-ParB$_{P1}$ and YFP-ParB$_{PMT1}$ (GL995). Fraction of cells in which *ori* and *ter* colocalized is indicated (inset); fluorescence profiles as in (C); demographs as in (C), signals oriented based on YFP-ParB$_{PMT1}$.

(legend continued on next page)

The Gram-negative bacterium *B. bacteriovorus* (a member of the recently proposed Bdellovibrionata phylum,[27] formerly considered as a δ-proteobacterium) features an extraordinary non-binary cell cycle (reviewed in Rotem et al.[28]) (Figure 1A). First, the mono-flagellated and fast-swimming attack phase (AP) cells search for prey in the environment. Upon pili-mediated attachment to a Gram-negative bacterium,[29] the predator invades the periplasm of its prey by sneaking through a narrow hole in the outer membrane and peptidoglycan.[30,31] Precise remodeling of the prey cell wall leads to rounding of the bdelloplast (i.e., the *Bdellovibrio*-infected prey bacterium) without altering its osmotic integrity[30,31]. Within the bdelloplast, *B. bacteriovorus* digests the prey content[32] and grows as a filament before producing a variable, even or odd number of daughter cells, by multiple synchronous division events.[33] Flagellated monoploid cells then exit the prey ghost[34] and resume the cycle.

The filamentous growth and multiple progeny of *B. bacteriovorus* raise unexplored fundamental questions regarding the orchestration of chromosome-related processes during the cell cycle.[35] What prevents AP cells from growing and replicating their DNA likely relies on a prey-triggered developmental switch[36] that remains to be elucidated at the molecular level. After prey invasion, the single circular chromosome of each predator cell[37] has to be copied and partitioned multiple times before releasing daughter cells, challenging the principle of temporal coupling between chromosome replication, segregation, and cell division.[38] Remarkably, chromosome replication must generate odd or even numbers, in contrast with common exponential multiplication patterns. Whereas a few hints suggest that *B. bacteriovorus* exploits multiple replisomes at the same time during its growth phase,[39,40] unambiguous insights into native replication dynamics are lacking. In addition, how and when chromosome segregation occurs relative to replication and cell division is unknown.

Here, we provide key insights into the spatial organization of the chromosome and the orchestration of chromosome replication and segregation during the intriguing life cycle of *B. bacteriovorus*. Using epifluorescence microscopy on living cells, followed by quantitative image analysis at the single-cell and population levels, we monitored the subcellular localization of *ori* and *ter* loci, as well as the native replication and segregation machineries, during the G1 (non-replicative), G1-S transition, and S (replicative) phases of the synchronized predatory cell cycle. Our results reveal the unusual polarity and compaction of its nucleoid, and shed light on a complex choreography of chromosome replication and ParABS-dependent segregation leading to the generation of a variable, even or odd number of offspring.

RESULTS

The chromosome of G1 predator cells features an unusual *ori-ter* polarity

To gain insight into the spatial organization of the chromosome in living *B. bacteriovorus* cells, we labeled the chromosomal origin (*ori*) and terminus (*ter*) using orthologous *parS*/ParB pairs[41]. Here, the $parS_{PMT1}$ or $parS_{P1}$ sequence (from *Yersinia pestis* or the P1 prophage, respectively) was integrated in the chromosome of the wild-type HD100 strain near to the predicted *ori* or *ter* locus, respectively (see STAR Methods), and fluorescent fusions to the cognate *parS*-binding proteins $ParB_{PMT1}$ and $ParB_{P1}$ were constitutively produced from a replicative plasmid (Figure 1B). We first monitored the subcellular position of *ori* (YFP-$ParB_{PMT1}$) or *ter* (CFP-$ParB_{P1}$) in living attack-phase (AP) cells, using epifluorescence microscopy. Each locus was detected as a single unipolar focus in most cells (Figures 1C and S1A), supporting the long-standing notion that AP cells carry only one copy of their chromosome and represent the non-proliferative (G1) phase of the cell cycle (Figure 1A).[5,28,40] Similar analyses of fluorescence profiles in a series of control strains (carrying non-cognate *parS*/ParB pairs and/or lacking the *parS* tag) confirmed that foci correspond to specific *parS*/ParB pairs (Figures S1B and S1C), consistent with previous locus labeling data obtained with this system in other species.[15,17,41–44] These reporters also localized at the cell poles when the corresponding ParB fusion was produced at lower levels from a *B. bacteriovorus* AP-specific promoter (Figures S2A and S2B), excluding artifacts from overproduction.[42] We found that *ori* and *ter* occupy opposite poles in the majority of the cells in which both loci were labeled (67% cells, n = 3,593 in a representative experiment) (Figure 1D). To determine the polarity of this *ori-ter* arrangement, we took advantage of RomR, an essential component of a predation complex at the invasive pole of *B. bacteriovorus* (Figure S2C).[45] Interestingly, the *ter* marker localized at the pole opposite a RomR-tdTomato fusion in most cells (79% cells, n = 6,061 in a representative experiment) (Figure 1E). Consistently, images of G1 *B. bacteriovorus* cells attached to *E. coli* cells showed that *ori* occupies the invasive, non-flagellated pole, whereas *ter* localizes at the flagellated pole in the majority of cells (Figures 1F and S2D). Additional evidence for this orientation was obtained using the sheathed unipolar flagellum[46] as a polarity beacon, labeled with membrane dyes in cells carrying the *ori* and/or *ter* labeling system (Figures 1G, S2E, and S2F). Taken together, these data show that in most G1 *B. bacteriovorus* cells, chromosomal *ori* and *ter* loci are positioned at the invasive and flagellated poles, respectively. Note that the preferential localization of *ter* is more flexible (at the flagellated pole in ~70% of cells regardless of the polar marker) compared to the strict localization of *ori* at the

(E) *ter* localizes at the pole opposite RomR in most cells. Left to right: representative phase contrast and fluorescence images of AP cells of *ter::*$parS_{P1}$ strain expressing RomR-TdTomato and CFP-$ParB_{P1}$ (GL816). Fraction of cells in which RomR and $ParB_{P1}$ colocalized is indicated (inset); fluorescence profiles as in (C); demographs as in (C), signal oriented based on RomR-tdTomato.

(F) *ori* occupies the invasive pole and *ter* occupies the flagellated pole during prey attachment. Representative phase contrast and fluorescence images of AP cells of *ori::*$parS_{PMT1}$ *ter::*$parS_{P1}$ strain expressing cognate CFP-$ParB_{P1}$ and YFP-$ParB_{PMT1}$ (GL995) 30 min after mixing with prey.

(G) *ori* occupies the non-flagellated pole and *ter* occupies the flagellated pole. Representative phase contrast and fluorescence images of AP cells of *ori::*$parS_{PMT1}$ *ter::*$parS_{P1}$ strain expressing cognate CFP-$ParB_{P1}$ and YFP-$ParB_{PMT1}$ (GL995) after staining with FM4-64. Arrowheads point at *ori* and *ter* foci at opposite poles.

(H) Histogram of the relative distance from fluorescent spot of RomR-TdTomato (red), CFP-$ParB_{P1}$ (cyan), and YFP-$ParB_{PMT1}$ (yellow) to the nearest cell pole for cells in (C) and (E); mean and SD values are shown. For all panels, schematics illustrate the relevant *ori* and *ter* labeling construct. Scale bars, 1 μm. n, number of cells analyzed in a representative experiment. For all, experiments were performed at least twice. For all panels, cell outlines were obtained with Oufti.
See also Figures S1 and S2.

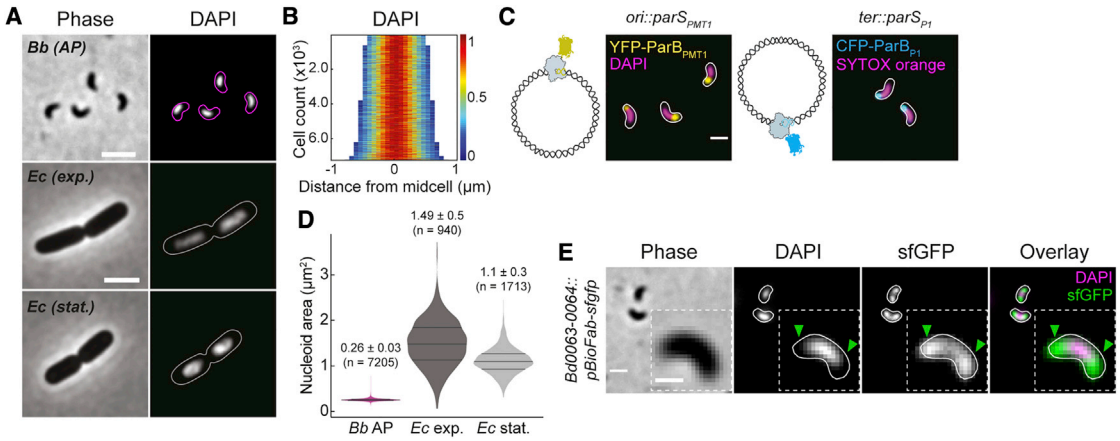

Figure 2. The nucleoid of *Bdellovibrio bacteriovorus* forms a dense meshwork that partially excludes freely diffusing proteins

(A) The chromosome of *B. bacteriovorus* forms a dense meshwork. From top to bottom: representative phase contrast and fluorescence images of fresh AP cells of wild-type (WT) *B. bacteriovorus* and of exponential and stationary phase cells of WT *E. coli* stained with DAPI (HD100 and MG1655, respectively). Scale bar, 2 μm.

(B) Demograph of the DAPI signal from *B. bacteriovorus* images in (A). Heatmap represent relative fluorescence intensities.

(C) *ori* and *ter* colocalize with the nucleoid tips. Representative overlay images of AP cells of *ori::parS*$_{PMT1}$ and *ter::terS*$_{P1}$ strains expressing cognate YFP-ParB$_{PMT1}$ or CFP-ParB$_{P1}$ (GL868 and GL771, respectively) stained with DAPI and SYTOX orange as indicated. Schematics illustrate the locus labeling construct. Scale bar, 1 μm.

(D) The nucleoid of *B. bacteriovorus* is more compacted than the one of *E. coli*. Violin plots of the nucleoid area distributions in WT *B. bacteriovorus* and exponential and stationary phase *E. coli* from cells in A. The lines indicate the 25, 50 and 75 percent quantiles, bottom to top, respectively. Mean and standard deviation values are shown on top of the corresponding plot. n indicate the number of cells analyzed in a representative experiment.

(E) The nucleoid of *B. bacteriovorus* partially excludes freely diffusing proteins. Representative phase contrast and fluorescence images of AP cells constitutively expressing *sfgfp* from the *Bd0063-0064* intergenic locus, *Bd0063-0064::pBioFab-sfgfp* (GL1212), stained with DAPI. Inset: enlarged example, arrowheads point to nucleoid exclusions. *pBioFab* is a synthetic promoter that is constitutively active. Scale bar is 1 μm except in the inset (0.5 μm). For all panels, cell outlines were obtained with Oufti.

See also Figure S3.

invasive pole. Strikingly, *B. bacteriovorus* features an inverse chromosomal polarity compared to other species carrying one (or more) unipolar flagellum, in which the chromosomal centromere is always located at the flagellated pole of newborn cells (e.g., *Caulobacter crescentus*,[11,47] *Vibrio cholerae*,[48] and *Agrobacterium tumefaciens*[16]).

The chromosome of *B. bacteriovorus* is packed in a dense nucleoid that partially excludes freely diffusing proteins

Demographs and fluorescence profiles representing the subcellular localization of *ori* and *ter* loci (Figure 1C) or the polar marker RomR (Figure 1E) suggest that *ori* and *ter* occupy slightly off-pole positions. Indeed, these loci were more distant from the closest cell pole than RomR (Figure 1H). This is consistent with the idea that the chromosome of *B. bacteriovorus* forms a nucleoid that does not fill the entire cytoplasm, as previously proposed.[49,50] Yet, this aspect of the *B. bacteriovorus* chromosome was never explored in living cells. Staining the DNA of G1 cells with fluorescent dyes confirmed the existence of a well-defined nucleoid occupying a fraction of the cytoplasm (Figures 2A, 2B, and S3A), with *ori* and *ter* foci marking the tips of the nucleoid (Figures 2C, S3B, and S3C).

Nucleoid area in G1 *B. bacteriovorus* cells is smaller than measurements reported in other species so far,[51] including *E. coli* (Figures 2A and 2D). Genome sizes of *B. bacteriovorus* and *E. coli* are roughly similar (3.8 Mb and 4.6 Mb, respectively), indicating that the chromosome meshwork is more compact in *B. bacteriovorus*. Remarkably, we found that freely diffusing fluorescent proteins were at least partially excluded from the *B. bacteriovorus* nucleoid (Figure 2E), regardless of the fluorescent protein or the DNA dye (Figures S3D and S3E). We hypothesize that this intriguing distribution might result from the highly condensed DNA network. Although it is well established that the mobility of large molecular complexes such as ribosomes,[52–54] protein aggregates,[51,55,56] or higher order assemblies[57,58] is impeded by nucleoids, this is the first report, to the best of our knowledge, of relatively small monomeric proteins being excluded.

Spatial arrangement of the chromosome is maintained during the G1-S transition and DNA replication initiates at the invasive pole

We subsequently set out to investigate chromosome dynamics further in the cell cycle when the predator cell resides within its prey, where it is expected to replicate its genomic content. To directly track DNA replication in living cells, we first monitored the subcellular distribution of DnaN, the replisome β-clamp commonly used as a proxy for replisome assembly and dynamics.[59] We designed a scarless *dnaN*::*dnaN-msfgfp* construct at the native chromosomal locus in a wild-type background, allowing the production of a DnaN-msfGFP fusion in place of the endogenous DnaN. DnaN-msfGFP signal was diffuse in the cytoplasm in G1 cells (exhibiting the partial nucleoid exclusion described above) (Figure 3A), indicative of unassembled replisome and consistent with the absence of DNA replication in G1. A DnaN-msfGFP focus appeared at one cell pole 95 ±

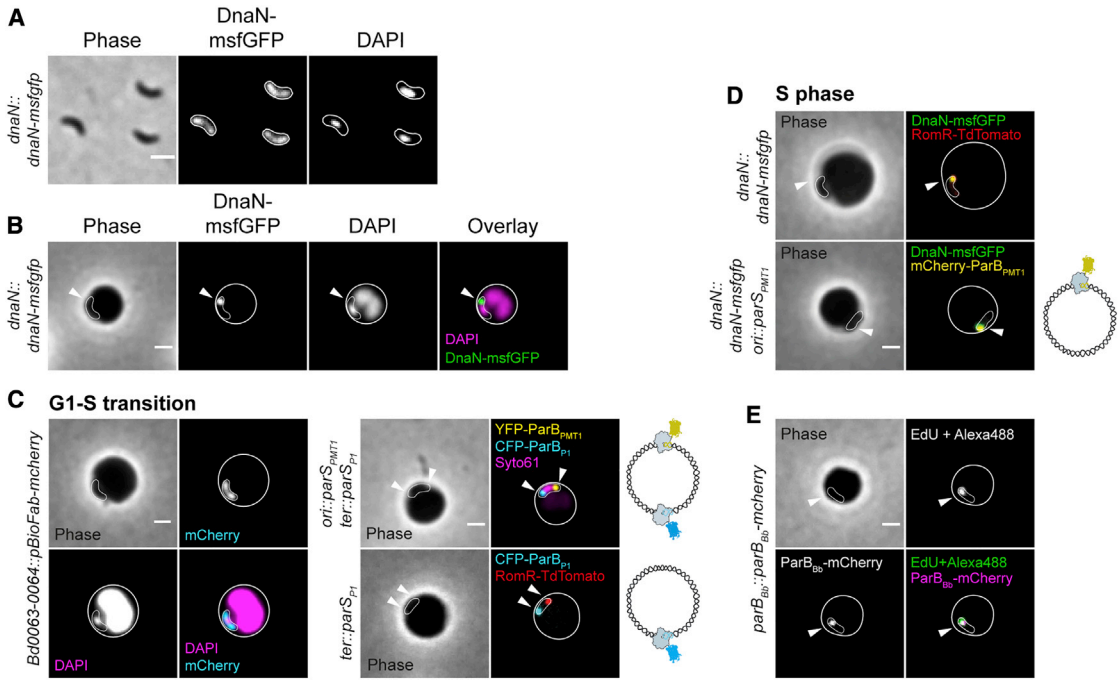

Figure 3. Chromosomal arrangement is maintained during the G1-S transition and DNA replication starts at the invasive pole

(A) DNA replication is inhibited in G1 phase and the diffuse DnaN signal exhibits partial nucleoid exclusion. Representative phase contrast and fluorescence images of AP cells of a *dnaN::dnaN-msfgfp* strain (GL673); cell outlines were obtained with Oufti.

(B) The replisome assembles at one cell pole. Representative phase contrast and fluorescence images of *dnaN::dnaN-msfgfp* strain (GL673) stained with DAPI 60 min after mixing with *E. coli* prey. Arrowhead points to the DnaN-msfGFP focus indicative of an active replisome.

(C) The chromosome of *B. bacteriovorus* is still compacted during G1-S transition and *ori-ter* polarity is maintained. Representative phase contrast and fluorescence images of (left) cells constitutively producing mCherry from a chromosomal locus, *Bd0063-0064::pBioFab-mcherry* (GL1025) stained with DAPI and imaged 30 min after mixing with *E. coli* prey, showing that the nucleoid does not expand to the cell poles unlike free mCherry used to visualize the whole cell; (right, top) *ori::parS*$_{PMT1}$ *ter::parS*$_{P1}$ strain expressing cognate CFP-ParB$_{P1}$ and YFP-ParB$_{PMT1}$ (GL995) stained with Syto61 and imaged 35 min after mixing with *E. coli* prey; *ori* and *ter* occupied opposite poles (arrowheads) in 71% of cells (n = 96 from one representative experiment); (right bottom) *ter::parS*$_{P1}$ strain expressing cognate CFP-ParB$_{P1}$ and RomR-TdTomato (GL816) imaged 35 min after mixing with *E. coli* prey; *ter* and RomR occupied opposite poles in 73% of cells (n = 77 from one representative experiment).

(D) DNA replication initiates at the invasive cell pole (start of the S phase). Representative phase contrast and fluorescence images of (top) *dnaN::dnaN-msfgfp* strain expressing RomR-TdTomato (GL1211) imaged 75 min after mixing with *E. coli* prey; colocalization in 98% of cells (n = 133 from one representative experiment); (bottom) *ori::parS*$_{PMT1}$ *dnaN::dnaN-msfgfp* strain expressing cognate mCherry-ParB$_{PMT1}$ (GL1103) imaged 75 min after mixing with *E. coli* prey; colocalization in 99% of cells (n = 104 from one representative experiment); Colocalization was quantified manually in (C) and (D).

(E) Colocalization of newly synthesized DNA and the *ori* region marked with the endogenous ParB$_{Bb}$ at the beginning of the S phase in *B. bacteriovorus.* Representative phase contrast and fluorescence images of cells of *parB*$_{Bb}$*::parB*$_{Bb}$*-mcherry* strain (GL906) 150 min after mixing with prey, exposed to a 5-min pulse of the nucleotide analog EdU, which was fluorescently labeled with Alexa488. ParB$_{Bb}$-mCherry was used to label *ori* since DnaN-msfGFP foci were unstable in this experimental setup. Arrowheads point to fluorescent foci. Schematics illustrate the *ori* and *ter* labeling construct used in each panel. *B. bacteriovorus* and bdelloplasts outlines in (B)–(E) were drawn manually based on the phase contrast images. Scale bars, 1 μm.

See also Figures S3 and S6F.

14 min after mixing with an *E. coli* prey cell (from 3 independent time-lapse experiments, total n = 318 bdelloplasts) (Figure 3B), marking replisome assembly and DNA replication initiation. We define the period between prey entry and initiation of DNA replication as the G1-S transition. During that period, the chromosome of *B. bacteriovorus* was still compact, and *ori-ter* polarity was maintained (Figure 3C). Importantly, we obtained several lines of evidence providing unambiguous support to the previously proposed idea that DNA replication initiates at the invasive pole[40]: (1) fluorescent foci of DnaN and RomR fusions occupied the same pole (98% cells, n = 133) (Figure 3D), (2) the DnaN-msfGFP focus colocalized with *ori* (Figure 3D), which was labeled either with *parS*$_{PMT1}$·YFP-ParB$_{PMT1}$ (colocalization in 99% cells, n = 104) (Figure 3D) or with the centromeric protein ParB$_{Bb}$ (see below; colocalization in 93% cells, n = 111) (Figure S5D), and (3) Click-labeling of the thymidine analog 5-ethynyl-2′-deoxyuridine (EdU) revealed a DNA synthesis spot that colocalized with the *ori* region (Figures 3E, S3G, and S3H). These results also validate the use of the *parS*$_{PMT1}$·ParB$_{PMT1}$ pair as proxy for the chromosomal *ori* in *B. bacteriovorus.* Thus, the spatial arrangement of the chromosome seen in G1 cells is preserved during the G1-S transition upon prey invasion.

Replisome dynamics reveal sequential firing of replication rounds and co-existence of multiple active replisomes in the growing predator

Examination of hundreds of predator cells imaged in time-lapse upon DNA replication initiation revealed common subcellular

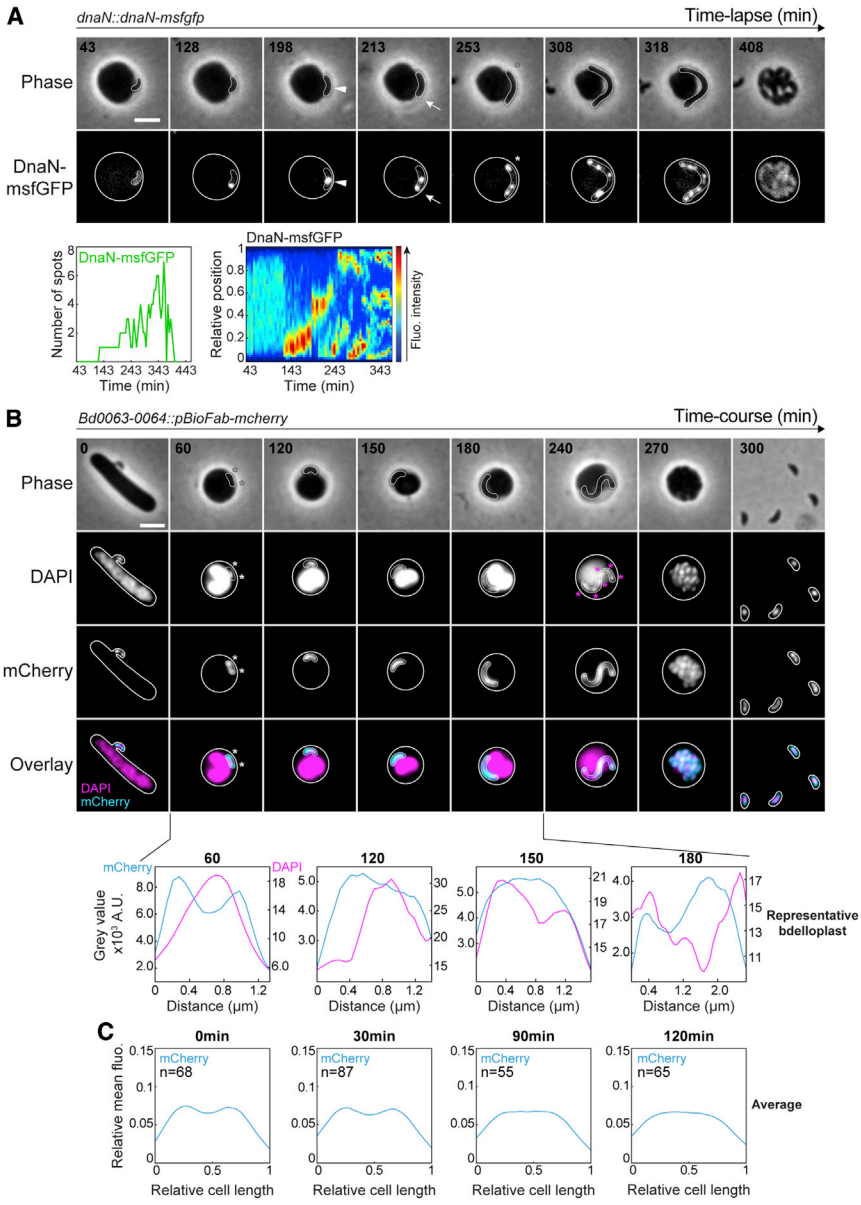

Figure 4. Multiple concomitant rounds of DNA replication in *B. bacteriovorus*

(A) Replisome dynamics during the proliferative (S) phase. *B. bacteriovorus* strain *dnaN::dnaN-msfgfp* (GL673) was mixed with prey and imaged in time-lapse after 43 min at 5-min intervals. Top: phase contrast and fluorescence images of selected time points of a representative experiment are shown. Arrowhead points to a mid-cell positioned DnaN-msfGFP focus; arrow points to the second DnaN-msfGFP focus; asterisk points to the third DnaN-msfGFP focus. The full time-lapse is shown in Video S1. Bottom: number of DnaN-msfGFP spots detected in Oufti over time (left) and kymograph of the DnaN-msfGFP signal along the cell length (right), for the same cell. Scale bar, 2 μm. See also Figure S6F.

(B and C) Loss of nucleoid exclusion suggesting chromosome decondensation during the proliferative (S) phase.

(B) Time-course experiment with strain *Bd0063-0064::pBioFab-mcherry* (GL1025). Cells were mixed with prey and stained with DAPI every 30 min, prior imaging. Top: phase contrast and fluorescence images of selected time points from a representative experiment are shown; white asterisks point to nucleoid exclusion of free mCherry at a time point prior DNA replication initiation; magenta asterisks point to clear nucleoid separation before cell division. Bottom: fluorescence intensity profiles of the corresponding signals in the same cells. Exclusion of mCherry from the DAPI signal is visible at 60 min but is less evident at 120- and 150-min. Scale bar, 2 μm. For all, outlines of *B. bacteriovorus* and bdelloplasts were drawn manually based on phase contrast images.

(C) Average pole-to-pole profiles of mean relative fluorescence intensity of mCherry for the indicated number of cells (n) at representative time points from the experiment described in (B). Exclusion of mCherry is visible at 0–30 min, but is not visible at 90 and 120 min when replication is ongoing.

See also Figure S4 and Video S1.

patterns. First, the DnaN-msfGFP focus migrated from the invasive pole to a midcell position (Figure 4A, arrowhead), likely reflecting the progression of replication along the mother chromosome.[60,61] A second DnaN-msfGFP focus was detected on average 167 ± 15 min post-mixing with prey (i.e., 71 ± 5 min after the first focus), usually at the invasive pole (in 73.9% of 318 bdelloplasts from 3 independent time-lapse experiments) (Figure 4A, arrow for one representative bdelloplast). Transient splitting or merging of foci was occasionally observed, possibly representing the two replication forks, as reported in *Caulobacter crescentus*.[62] A third DnaN-msfGFP spot formed at the opposite pole (Figure 4A, asterisk), followed by additional DnaN-msfGFP foci, which showed highly dynamic movements, indicating that more than two replisomes are simultaneously active in the growing predator cell (Video S1). The replication initiation steps do not seem to follow a readily predictable spatiotemporal pattern beyond the first two rounds, and new DnaN foci usually appeared sequentially instead of simultaneously, suggesting asynchronous firing of replication initiation (Figure 4A; Video S1). Similar dynamics were obtained when a fluorescent fusion of the clamp-loader component DnaX was used to label the replisome, as done in other species,[63–66] although the signal intensity of DnaX-msfGFP (replacing the native DnaX, *dnaX::dnaX-msfgfp*) was weaker than the DnaN fusion (Figure S4A). The gyrase inhibitor novobiocin, which specifically blocks DNA replication initiation,[67] prevented the formation of the first or subsequent DnaN-msfGFP foci depending on when the drug was added in the course of the cell cycle (Figure S4B). Thus, the growing number of replisomes during the S-phase shows that multiple rounds of DNA replication can occur concomitantly, and we hypothesize that these initiated asynchronously.

Nucleoid decompaction may occur after DNA replication initiation

Dynamic replication factories (Figure 4A) need access to the chromosome, raising the question of whether nucleoid compaction might change upon G1/S transition. To gain insight into nucleoid dynamics during growth inside the prey, we imaged DAPI-stained cells of a strain constitutively producing free mCherry (to label the whole predator cell), during a time-course of prey infection. Early after DNA replication initiation, the nucleoid still occupied a restricted area in the cell from which the mCherry signal was partially excluded (Figures 4B, 4C, and S4C). At later stages (when multiple replisomes had been observed) (Figure S4C), the mCherry and DAPI signals overlapped without obvious exclusion pattern, suggesting an expansion of the chromosome meshwork compatible with mCherry diffusion (Figures 4B and 4C). Of note, areas that were the least stained with DAPI, presumably corresponding to regions of lower DNA density, were often occupied by a DnaN-msfGFP-labeled replisome (Figure S4C, arrowheads). Nucleoid segregation and, conceivably, re-compaction of the chromosomes (marked by distinct DAPI-stained units) was visible at late time point's prior division (Figures 4B, asterisks, and S4C, arrowheads). Based on these observations, we propose that nucleoid de-condensation might occur in growing *Bdellovibrio* cells, possibly triggered by the progression of replisomes and followed by re-compaction of the chromosomes before cell division.

Duplicated *ori* undergo asymmetric polar segregation and *ter* segregation is uncoupled from cell division

The simultaneous occurrence of multiple replication events in the growing predator cell raises the question of how and when the newly synthesized chromosomes are segregated. Because the subcellular positions of *ori* and *ter* loci determine the dynamics of chromosome segregation in other species[7], we examined the spatial arrangement of the chromosome during the proliferative (S) phase of the cell cycle. Time-lapse imaging of labeled *ori* showed that a second focus appeared and quickly moved toward the opposite pole (Figures 5A and S5A; Video S2), reminiscent of the asymmetric *ori* segregation described in several binary-dividing species.[11,15,17,18,68,69] In line with this model,[24,47] the *ter* focus shifted from its polar position to midcell (Figures 5B and S5B). Interestingly, this first round of *ter* segregation was achieved to completion, as the *ter* copies clearly split in two distinct foci at midcell (Figures 5B; Video S3). Thus, *ter* segregation is temporally uncoupled from cell constriction.

To further investigate segregation dynamics, we turned to the endogenous ParB (here named $ParB_{Bb}$) to mark the native centromeric $parS_{Bb}$ site located next to *ori* (Figure S1A). Consistent with the reported biphasic expression pattern of the corresponding operon,[70,71] we could only detect weak fluorescent signal in G1 cells of a strain in which $parB_{Bb}$ was replaced by $parB_{Bb}$-*mcherry* (Figure S5C). Nevertheless, although no detectable foci could be observed in the G1 phase (see below), $ParB_{Bb}$-mCherry always formed a focus that colocalized with the first DnaN-msfGFP-labeled replisome (Figure S5D). This is consistent with the colocalization of DnaN and *ori* shown previously. Furthermore, the first duplication and polar segregation of $ParB_{Bb}$-mCherry foci showed similar dynamics as $parS_{PMT1}$·YFP-$ParB_{PMT1}$-labeled *ori* (Figures 5C, 5D, and S5E) supporting our previous finding of asymmetric *ori* segregation and the use of $parS_{PMT1}$·YFP-$ParB_{PMT1}$ and $ParB_{Bb}$-mCherry as reliable *ori* reporters. Monitoring the dynamics of both $ParB_{Bb}$ and *ter* in the same cells showed that *ter* relocation to midcell started after the newly duplicated *ori* reached the non-invasive pole (Figure 5E, time point, 200 min).

Chromosome segregation occurs progressively as new copies are being synthesized

After the first "binary-like" replication and segregation round, additional $ParB_{Bb}$ foci gradually appeared (Figures 5C and 5D). The highest number of $ParB_{Bb}$ foci varied between bdelloplasts and reached 5 on average under these conditions (n = 69, representative time-lapse experiment) (Figure 5C). As expected, the $ParB_{Bb}$-mCherry foci always colocalized with YFP-$ParB_{PMT1}$-labeled *ori* on snapshots taken at various times during the proliferative phase of the cell cycle (Figure S5E). Strikingly, $ParB_{Bb}$ foci were always evenly distributed during filamentous growth (Figure 5C; Video S4), indicating that even after the first round of replication, *ori* segregation occurs as soon as new chromosomal copies are being synthesized. In addition, temporal uncoupling of *ter* segregation from cell division was not limited to the first replication round, as additional *ter* foci appeared before visible cell constriction (Figure S5B, asterisks). We did not observe *ter* foci at the poles of the growing cell, unlike *ori* foci (Figures 5C and S5B, asterisk), hinting that *ori* but not *ter* will occupy the two "old" poles transmitted from the mother cell to the progeny. In the last minutes before non-binary cell division, *ter*-associated signal dispersed, and foci reappeared in the progeny (Figure S5B), which could suggest a temporary reorganization of the *ter* macrodomain during the division process.

Perturbations in the ParABS system impact progressive *ori* segregation and accurate cell-cycle progression

The asymmetric pole-to-pole segregation of the first duplicated centromere and the progressive partitioning of additional copies strongly suggest that the ParAB*S* system drives these segregation events in *B. bacteriovorus*. To examine this idea further, we introduced perturbations in that system by constitutively producing $ParB_{Bb}$ fusions from a plasmid that is expected to modify the ParA:ParB interplay.[72,73] Overproduced $ParB_{Bb}$-FP fusions formed distinct foci in predator cells after prey invasion (Figure 6A, arrowhead), which colocalized with the YFP-$ParB_{PMT1}$-labeled *ori* copies (Figure S6A). However, the localization pattern of these $ParB_{Bb}$·*ori* complexes (Figure 6A, asterisks) differed from cells in which $ParB_{Bb}$ is produced at native levels, consistent with segregation defects: (1) in longer cells the second $ParB_{Bb}$ focus rarely reached the opposite pole and instead stalled in the middle of the cell (Figures 6A and 6B), and (2) the number of foci did not regularly increase before division, and fusions of existing foci were observed (Figure 6A, time point 290 min). Moreover, constitutive production of $ParB_{Bb}$, either untagged or in fusion with mCherry or msfGFP, led to pronounced phenotypes in the released progeny: (1) they displayed more variable and on average larger cell length and nucleoid area than control strains (Figures 6C, S6B, and S6C), and (2) cells had aberrant numbers of *ori* foci (Figure S6D). Altogether, our

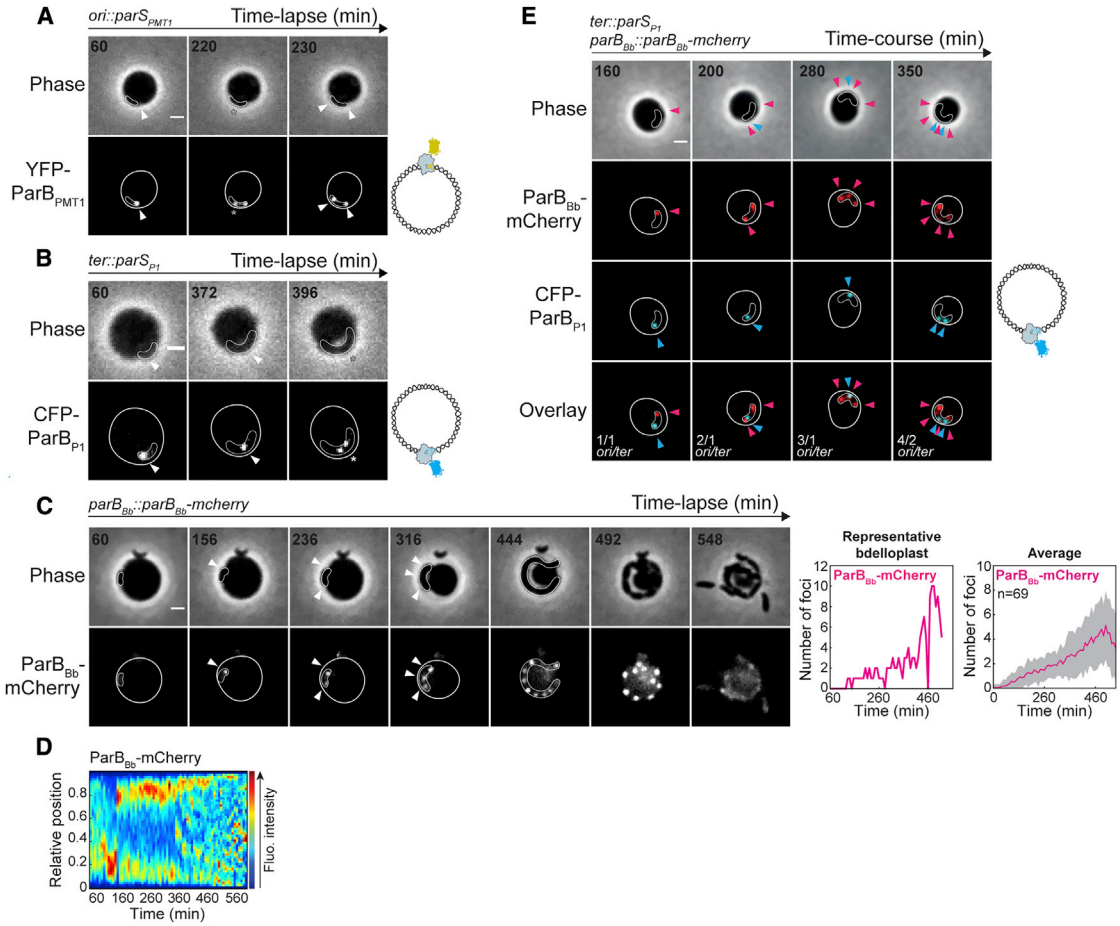

Figure 5. Spatio-temporal arrangement of the chromosome during the proliferative phase of the cell cycle in *B. bacteriovorus*

(A) First round of *ori* segregation is asymmetric. *B. bacteriovorus* strain *ori::parS$_{PMT1}$* expressing cognate YFP-ParB$_{PMT1}$ (GL868) was mixed with prey and imaged in time-lapse after 60 min with 10-min intervals. Phase contrast and fluorescence images of selected time points are shown; arrowheads point to the *ori* focus before replication and the duplicated *ori* foci after segregation; asterisk points to the *ori* copy being segregated toward the opposite pole. The time-lapse is shown in Video S2.

(B) *ter* segregation is temporally uncoupled from cell division. *B. bacteriovorus* strain *ter::parS$_{P1}$* expressing cognate CFP-ParB$_{P1}$ (GL771) was mixed with prey and imaged in time-lapse after 60 min with 8-min intervals. Phase contrast and fluorescence images of selected time points are shown; arrowhead and asterisk point to mid-cell *ter* localization and segregation, respectively. The time-lapse is shown in Video S3.

(C) ParB-driven *ori* segregation during S phase. *B. bacteriovorus* strain *parB$_{Bb}$::parB$_{Bb}$-mcherry* (GL906) was mixed with prey and imaged in time-lapse after 60 min with 8-min intervals. Left: phase contrast and fluorescence images of selected time points are shown. Arrowheads point to the first ParB$_{Bb}$-mCherry focus, two segregated ParB foci, then 3 segregated foci; multiple well-separated ParB$_{Bb}$-mCherry foci are visible at time-point 444 min. The time-lapse is shown in Video S4. Right: number of ParB$_{Bb}$-mCherry spots detected in Oufti over time, for the same representative bdelloplast; average number of ParB$_{Bb}$-mCherry spots detected in Oufti, over time; gray area indicates SD; n indicates the average number of bdelloplasts analyzed until time point 384 min, from which the number of bdelloplasts that could be analyzed progressively decreased to 62.

(D) Kymograph of the ParB$_{Bb}$-mCherry signal along the cell length for one representative cell. Arrowheads indicate timing of, from left to right, the first ParB$_{Bb}$-mCherry focus, pole-to-pole segregation upon duplication, and the third focus.

(E) *ter* relocation to mid-cell starts after the second *ori* reaches the non-invasive pole. *B. bacteriovorus* strain *parB$_{Bb}$::parB$_{Bb}$-mcherry ter::parS$_{P1}$* expressing cognate CFP-ParB$_{P1}$ (GL1368) was mixed with prey and imaged in time-course with 30-min intervals. Phase contrast and fluorescence images of selected time points are shown; pink arrowheads point to *ori* copies; blue arrowheads point to *ter* copies. Schematics illustrate the *ori* and *ter* labeling constructs used in each panel. Scale bars, 1 μm. For all, outlines of *B. bacteriovorus* and bdelloplasts were drawn manually based on phase contrast images.

See also Figure S5 and Videos S2, S3, and S4.

data are consistent with the idea that the ParABS system is required to achieve multiple progressive rounds of asymmetric *ori* segregation in *B. bacteriovorus*. Of note, nucleoid exclusion of cytoplasmic proteins was still observed in ParB$_{Bb}$-overexpressing cells, hinting that the mechanism of chromosome compaction is independent of ParABS-mediated chromosome segregation (Figure S6E).

ParB$_{Bb}$ binds the chromosomal centromere only after replication initiation

During these experiments, we surprisingly noticed that overproduced fluorescent ParB$_{Bb}$ fusions displayed a strong cytoplasmic signal but no focus in G1 cells (Figure S6B), suggesting that the above-mentioned absence of natively produced ParB$_{Bb}$-mCherry focus (Figure S5C) could not be solely explained by low

CellPress
OPEN ACCESS

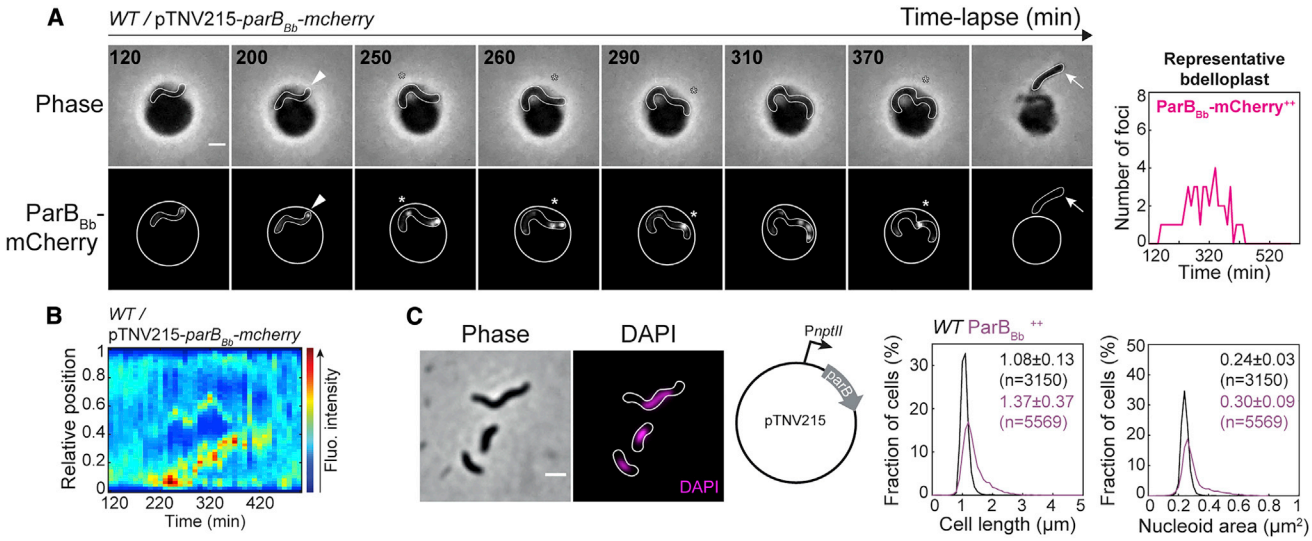

Figure 6. The ParABS system contributes to progressive *ori* segregation

(A) Overproduction of $ParB_{Bb}$ leads to chromosome segregation defects. *B. bacteriovorus* strain *WT*/pTNV215-*parB*$_{Bb}$-*mcherry* (GL1002) was mixed with prey and imaged in time-lapse after 120 min with 10-min intervals. Left: phase contrast and fluorescence images of selected time points; arrowhead points to a $ParB_{Bb}$-mCherry focus; asterisks point to altered *ori* behavior during the cycle; arrow points to a long daughter cell. Right: number of $ParB_{Bb}$-mCherry spots detected in Oufti, over time for the same representative bdelloplast.

(B) Kymograph of the $ParB_{Bb}$-mCherry signal along the cell length for the same representative bdelloplast as in (A).

(C) Overproduction of $ParB_{Bb}$ leads to phenotypic changes in AP cells. From left to right: representative phase contrast and fluorescence images of AP cells of a *WT* strain constitutively expressing untagged $ParB_{Bb}$ (GL1261) stained with DAPI; histograms of cell length and nucleoid area for the same strain (purple) compared to *WT* (black); mean and SD values are shown. n indicates the number of cells analyzed for each strain in a representative experiment. Scale bars, 1 μm. Outlines of *B. bacteriovorus* and bdelloplasts were drawn manually based on phase contrast images except in (C) where they were obtained with Oufti. Experiments were performed at least twice.

See also Figure S6.

protein amounts. This finding raises the intriguing hypothesis that endogenous $ParB_{Bb}$ is unable to accumulate at $parS_{Bb}$ sites during the G1 phase of the cell cycle. To get spatiotemporal insight into $ParB_{Bb}$ focus formation relative to cell-cycle progression, we constructed a strain producing both DnaN-msfGFP and $ParB_{Bb}$-mCherry as single copies from their native chromosomal locus. $ParB_{Bb}$ does not localize at $parS_{Bb}$ sites before the onset of DNA replication in *B. bacteriovorus* because the $ParB_{Bb}$-mCherry signal formed a first detectable focus after DnaN-msfGFP (41 min on average, from single-cell analysis in double-labeled strains, Figure 7A; or when comparing population averages of single-labeled strains, Figures S6F and S6G; note some cell-to-cell variability, Figures S6F and S6G). However, $ParB_{Bb}$ does not require an active replisome to sustain accumulation at $parS_{Bb}$, because we could still detect $ParB_{Bb}$-mCherry foci at the end of the S phase when the DnaN-msfGFP foci disassembled (Figure 7A). The $ParB_{Bb}$-mCherry signal became diffuse after cell constriction started (Figures 5C and 7A), consistent with the absence of focus in G1 cells. Thus, our data show that in *B. bacteriovorus*, $ParB_{Bb}$ does not accumulate on its cognate $parS_{Bb}$ sites during the G1 phase and G1/S transition.

Multiple *ori* copies serve as platforms for replication rounds

Finally, we asked how multiple chromosome replication events were orchestrated over time in growing *B. bacteriovorus* cells (i.e., whether DNA replication initiation steps were biased toward a specific subset of *ori* copies). Observation of bdelloplasts imaged in time-lapse showed that a DnaN-msfGFP spot colocalized with a $ParB_{Bb}$-mCherry-labeled *ori* at several places in the cell (n = 65 in a representative experiment) (Figure 7A, asterisks), suggesting that distinct *ori* loci can serve as replication initiation platforms. Although several DnaN-msfGFP foci often clustered near the cell ends (Figure 7A, see Discussion), distinct foci were observed in other cell regions. Consistently, the *ori* copies marked by both $ParB_{Bb}$-mCherry and DnaN-msfGFP (probably representing *ori* being replicated) occupy diverse subcellular positions and vary in number over time and among bdelloplasts (Figure 7A). Altogether, our data prompt us to propose that the asynchronous initiation of DNA replication from different *ori* platforms results in a non-exponential increase of chromosome numbers, consistent with odd or even numbers of daughter cells being released at each generation (Figure 7B).

DISCUSSION

In this study, we benchmarked the use of key fluorescent reporters to monitor the subcellular dynamics of chromosomal loci as well as the replication and segregation machineries in living *B. bacteriovorus* cells. Semi-automated analysis of intracellular features at the single-cell and population levels allowed us to shed light on how the chromosome is organized in space and time during the cell cycle, opening the way for future quantitative cell biological approaches in this bacterium. Taken together, our data suggest a model (Figure 7B) in which asynchronous initiation of multiple DNA replication rounds is sufficient to elucidate why

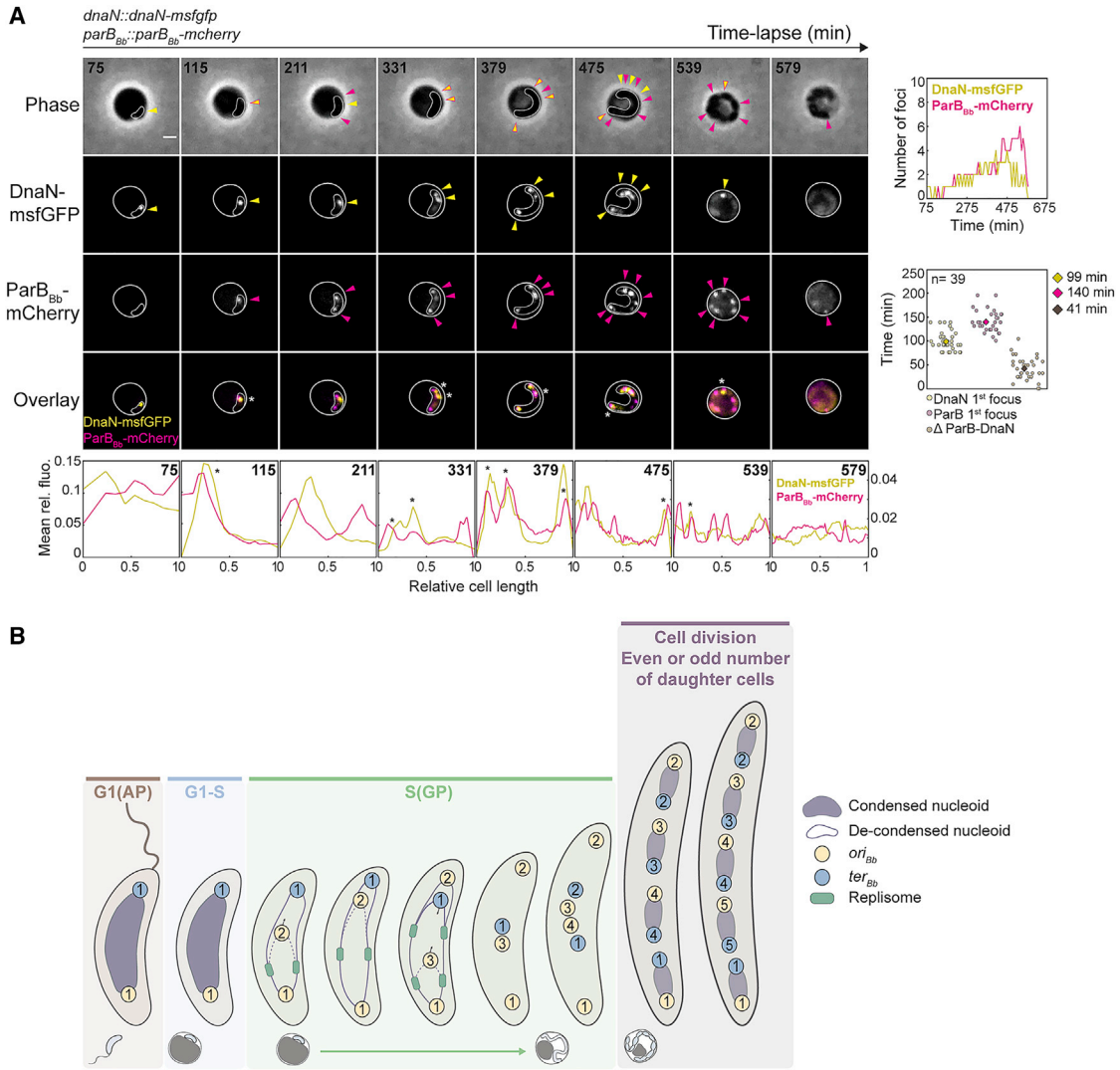

Figure 7. Stochastic chromosome replication initiation at multiple *ori* and progressive segregation producing odd or even offspring

(A) $ParB_{Bb}$ forms foci after DNA replication initiation and multiple copies of *ori* can serve as a template for the next replication round. *B. bacteriovorus* strain *dnaN::dnaN-msfgfp* $parB_{Bb}$*::*$parB_{Bb}$*-mcherry* (GL1055) was mixed with prey and imaged in time-lapse after 75 min with 8-min intervals. Top: left: phase contrast and fluorescence images of selected time points are shown. Arrowheads point to fluorescent foci; asterisks and two-colored arrowheads point to colocalization of the corresponding fluorescence signals; right: number of DnaN-msfGFP (yellow) and $ParB_{Bb}$-mCherry (pink) spots detected in Oufti, over time for the same representative bdelloplast; SuperPlot representation of the time of appearance of first DnaN-msfGFP and $ParB_{Bb}$-mCherry foci and the time difference between them, in single cells of the GL1055 strain; the average for each signal is represented as a colored diamond; n indicates the number of cells analyzed in this experiment. Bottom: mean pole-to-pole profiles of relative fluorescence intensity of the corresponding fusions in the same cells; asterisks point to colocalization of the corresponding fluorescence signals. Scale bar, 1 μm. Outlines of *B. bacteriovorus* and bdelloplasts were drawn manually for display based on phase contrast images.

(B) A model for non-binary chromosome choreography in *B. bacteriovorus.* The highly condensed nucleoid of G1 (AP) cells is arranged such that *ori* (yellow) occupies the invasive pole, and more flexible *ter* (blue) occupies the flagellated pole. Once inside the prey, cells experience a G1-S transition during which the state of the chromosome is apparently unchanged. At the beginning of the proliferative S (GP) phase, DNA replication starts from the invasive pole and the duplicated *ori* is segregated asymmetrically. Nucleoid visibly decondenses after DNA replication initiation. When the 2nd *ori* reaches the opposite pole, the replisome is at mid-cell. The 1st *ter* then moves from pole to mid-cell where it colocalizes with the 3rd *ori* copy, which was newly synthesized and segregated (usually from the same invasive pole). Progressive *ori* and *ter* segregations continue, following new DNA replication rounds where variable numbers and copies of *ori* serve as initiation platform, leading to odd or even ploidy. Distinct nucleoids are visible again before division of the mother cell by multiple fission. Nucleoid schematic for last two cells in S phase is omitted for clarity.

See also Figure S6.

chromosome copies do not necessarily double at each replication round, leading to variable, odd or even numbers. Indeed, although several chromosomes simultaneously served as replication templates, usually not all chromosomal copies present in the cell were being copied at the same time. The observation that the invasive pole hosts the second round of replication in ~70% of cells

suggests that the "mother" *ori* present at this pole is somehow primed, favoring re-initiation of chromosome replication at this location compared to the newly synthesized *ori*. Consistent with this idea, additional replisomes often accumulated from that pole in the growing predator, and later from the opposite pole, although DnaN foci were observed in other regions of the cell as well. What governs such spatial organization of DNA replication remains to be discovered. Considering the importance of transmitting a single and complete chromosome to each daughter cell, the dynamics of replication initiation are likely not determined by chance. We think that complex regulation occurs in both space and time to prevent replication from all *ori*s at the same time, and most importantly to avoid starting new synthesis that would prematurely end when prey resources are exhausted. Even though the temporal control of the S phase with respect to cell-cycle progression and synchronous divisions is still unclear, our data provide clues into this question as we show that the late steps of chromosome segregation and cell division are uncoupled. In line with this idea, the positioning of one *ori* at both old poles of the pre-divisional mother cell inevitably results in at least one septum not being placed between two *ter* copies (Figure 7B).

Our study also revealed insights into the spatial organization of *B. bacteriovorus* cells. First, the *ori* locus was always located near the invasive, non-flagellated pole of G1 *B. bacteriovorus* cells, in contrast with the chromosomal orientation in previously characterized mono-flagellated bacteria.[11,16,47,48] Based on RomR and flagellum labeling experiments, we conclude that the fraction of cells (~30%) in which *ori* and *ter* colocalized correspond to cases where *ter*, but not *ori*, is "misplaced." Whether the occasional presence of *ter* at the invasive pole results from to the relative flexibility of the *ter* macrodomain (reported in *E. coli*[74,75]) or from another aspect related to non-binary proliferation remains to be discovered.

Second, the relatively small area occupied by the nucleoid in G1 *B. bacteriovorus* cells indicates a dense chromosome meshwork. The unexpected non-homogeneous distribution of all freely diffusing fluorescent proteins that we tested showed partial exclusion from the DNA-containing region. So far, only larger objects were reported to be partially or fully excluded from the nucleoid (e.g., ribosomes or protein aggregates in *E. coli*[51–56]). Although these observations suggest that the compact DNA network constraints the mobility of small proteins in *B. bacteriovorus*, we cannot exclude that additional factors contribute to this phenomenon. Nevertheless, our observation that a free fluorescent protein is no longer nucleoid-excluded during the S phase is compatible with the idea of nucleoid decondensation. This would be consistent with higher chromosome processing activities during growth (including DNA replication but also transcription[70,76]), which may remodel the nucleoid and/or require increased accessibility within the nucleoid. The dynamics of chromosome compaction and decompaction at the single-cell level, the architecture of the chromosome and the physiological impact of nucleoid condensation on the *B. bacteriovorus* cell cycle remain to be investigated.

Finally, we found that $ParB_{Bb}$ is unable to accumulate at the *ori* region during the G1 and G1-S transition stages, even when produced constitutively. The detection of $ParB_{Bb}$ foci after DnaN foci suggests that DNA replication initiation might open up the *ori* region, allowing $ParB_{Bb}$ binding. It would be tempting to speculate that the accessibility of $parS_{Bb}$ may vary during the cell cycle depending on the level of nucleoid compaction; however, the heterologous $parS_{PMT1}$ inserted near endogenous $parS_{Bb}$ sites remained accessible to $ParB_{PMT1}$ at all times. To the best of our knowledge, this is the first example of a ParB homolog that does not permanently localize at the chromosomal centromere, regardless of protein levels, hinting that beside transcriptional modulation[70,71], $ParB_{Bb}$ function could be subjected to novel cell-cycle-dependent regulation. Detailed mechanistic investigation of the ParABS system in *Bdellovibrio,* including the analysis of ParA subcellular dynamics, should reveal interesting features of this highly conserved partitioning machinery.

Altogether, our data illustrate that *Bdellovibrio* is a treasure-trove for future discoveries of novel cell-cycle regulation and cellular organization strategies. Moreover, our study sets the path for using *B. bacteriovorus* as a model to expand the quantitative investigation of subcellular events in bacteria and highlights the exploitation of conserved proteins to address the needs of complex non-binary reproduction.

STAR★METHODS

Detailed methods are provided in the online version of this paper and include the following:

- KEY RESOURCE TABLE
- RESOURCE AVAILABILITY
  - Lead contact
  - Materials availability
  - Data and code availability
- EXPERIMENTAL MODEL AND SUBJECT DETAILS
  - Strains
  - Locus tags of genes used in this study
  - Labeling of *ori* and *ter*
  - Routine culturing of *B. bacteriovorus* and *E. coli*
- METHOD DETAILS
  - Plasmid conjugation by mating
  - EdU labeling of newly synthesized DNA
  - Live-cell imaging
  - Image acquisition
  - Image processing
  - Western blot analysis
  - Killing curves
  - SYBR Green normalization of predator density
- QUANTIFICATION AND STATISTICAL ANALYSIS
  - Cell, nucleoid and spot detection from images
  - Quantitative image analysis from cell meshes
  - Kymographs and demographs
  - Fluorescence profiles
  - Fluorescence spot position and intensity analysis
  - Nucleoid size measurement
  - Cell Projections using BactMAP
  - Killing curve analysis
  - Statistical analyses

SUPPLEMENTAL INFORMATION

Supplemental information can be found online at https://doi.org/10.1016/j.cub.2021.06.024.

ACKNOWLEDGMENTS

We are grateful to Charles de Pierpont for excellent technical support, Elodie Buche for the construction of the pMQ414-romR plasmid and GL512 strain, all members of the Laloux lab for stimulating discussions, Dr. Michaël Deghelt for insightful discussions and critical review of the manuscript, Dr. Seung-Hyun Cho and Kilian Dekoninck for advice on Western blots, Dr. Paula Montero Llopis for helpful advices on microscopy setups at the initiation of this project, Prof. Xavier De Bolle for sharing *parS*/ParB constructs, Prof. Liz Sockett for providing the HD100 strain, Prof. Daniel Kadouri for the pMQ414 plasmid, Prof. Edouard Jurkevitch for the pPROBE-NT plasmid, Prof. Christine Jacobs-Wagner for sharing the unpublished CJW6321 strain, Dr. Sarah Bigot for the construction of pBG18, Dr. Christian Lesterlin for sharing the plasmid, Prof. Leendert Hamoen and Prof. Tanneke den Blaauwen for sharing pTNV143, pTNV162, and pTNV167 plasmids, and Dr. Pauline Leverrier and Boris Stojilković for critical reading of the draft. J.K. is a Research Fellow (Aspirant) of the F.R.S.-FNRS, T.L. is a FRIA grantee of the F.R.S.-FNRS. G.L. is a Research Associate (Chercheur Qualifié) of the F.R.S.-FNRS. This work was supported by the European Commission (ERC starting grant PREDATOR 802331) and the F.R.S. - FNRS (Mandat d'Impulsion Scientifique-F.4521.18).

AUTHOR CONTRIBUTIONS

J.K. and T.N.V.S. performed experiments. J.K., T.N.V.S., and G.L. analyzed the data. J.K. prepared final figures. S.K.G., J.K., and G.L. optimized Oufti parameters for attack phase cell, nucleoid, and bdelloplast detection. S.K.G. advised on image analysis. G.L. wrote MATLAB codes for analysis of Oufti cell meshes. R.v.R. designed the cell projection workflow. O.R. designed the SybrGreen normalization assay. T.L. designed the killing curves analysis. G.L. supervised the work, acquired funding, and drafted the manuscript. All authors edited the manuscript.

DECLARATION OF INTEREST

The authors declare no competing interests.

Received: January 20, 2021
Revised: May 13, 2021
Accepted: June 9, 2021
Published: July 12, 2021

REFERENCES

1. Mahone, C.R., and Goley, E.D. (2020). Bacterial cell division at a glance. J. Cell Sci. *133*, jcs237057.
2. Angert, E.R. (2005). Alternatives to binary fission in bacteria. Nat. Rev. Microbiol. *3*, 214–224.
3. Jakimowicz, D., and van Wezel, G.P. (2012). Cell division and DNA segregation in Streptomyces: how to build a septum in the middle of nowhere? Mol. Microbiol. *85*, 393–404.
4. Waterbury, J.B., and Stanier, R.Y. (1978). Patterns of growth and development in pleurocapsalean cyanobacteria. Microbiol. Rev. *42*, 2–44.
5. Sockett, R.E. (2009). Predatory lifestyle of Bdellovibrio bacteriovorus. Annu. Rev. Microbiol. *63*, 523–539.
6. Surovtsev, I.V., and Jacobs-Wagner, C. (2018). Subcellular organization: A critical feature of bacterial cell replication. Cell *172*, 1271–1293.
7. Wang, X., Montero Llopis, P., and Rudner, D.Z. (2013). Organization and segregation of bacterial chromosomes. Nat. Rev. Genet. *14*, 191–203.
8. Webb, C.D., Teleman, A., Gordon, S., Straight, A., Belmont, A., Lin, D.C., Grossman, A.D., Wright, A., and Losick, R. (1997). Bipolar localization of the replication origin regions of chromosomes in vegetative and sporulating cells of B. subtilis. Cell *88*, 667–674.
9. Yang, M.C., and Losick, R. (2001). Cytological evidence for association of the ends of the linear chromosome in Streptomyces coelicolor. J. Bacteriol. *183*, 5180–5186.
10. Li, Y., Sergueev, K., and Austin, S. (2002). The segregation of the Escherichia coli origin and terminus of replication. Mol. Microbiol. *46*, 985–996.
11. Viollier, P.H., Thanbichler, M., McGrath, P.T., West, L., Meewan, M., McAdams, H.H., and Shapiro, L. (2004). Rapid and sequential movement of individual chromosomal loci to specific subcellular locations during bacterial DNA replication. Proc. Natl. Acad. Sci. USA *101*, 9257–9262.
12. Yamaichi, Y., Fogel, M.A., and Waldor, M.K. (2007). par genes and the pathology of chromosome loss in Vibrio cholerae. Proc. Natl. Acad. Sci. USA *104*, 630–635.
13. Lin, L., Osorio Valeriano, M., Harms, A., Søgaard-Andersen, L., and Thanbichler, M. (2017). Bactofilin-mediated organization of the ParABS chromosome segregation system in Myxococcus xanthus. Nat. Commun. *8*, 1817.
14. Espéli, O., Mercier, R., and Boccard, F. (2008). DNA dynamics vary according to macrodomain topography in the E. coli chromosome. Mol. Microbiol. *68*, 1418–1427.
15. Deghelt, M., Mullier, C., Sternon, J.-F., Francis, N., Laloux, G., Dotreppe, D., Van der Henst, C., Jacobs-Wagner, C., Letesson, J.-J., and De Bolle, X. (2014). G1-arrested newborn cells are the predominant infectious form of the pathogen Brucella abortus. Nat. Commun. *5*, 4366.
16. Ehrle, H.M., Guidry, J.T., Iacovetto, R., Salisbury, A.K., Sandidge, D.J., and Bowman, G.R. (2017). Polar Organizing Protein PopZ Is Required for Chromosome Segregation in Agrobacterium tumefaciens. J. Bacteriol. *199*, e00111-17.
17. Dubarry, N., Willis, C.R., Ball, G., Lesterlin, C., and Armitage, J.P. (2019). In Vivo Imaging of the Segregation of the 2 Chromosomes and the Cell Division Proteins of Rhodobacter sphaeroides Reveals an Unexpected Role for MipZ. mBio *10*, e02515-18.
18. Jung, A., Raßbach, A., Pulpetta, R.L., van Teeseling, M.C.F., Heinrich, K., Sobetzko, P., Serrania, J., Becker, A., and Thanbichler, M. (2019). Two-step chromosome segregation in the stalked budding bacterium Hyphomonas neptunium. Nat. Commun. *10*, 3290.
19. Livny, J., Yamaichi, Y., and Waldor, M.K. (2007). Distribution of centromere-like parS sites in bacteria: insights from comparative genomics. J. Bacteriol. *189*, 8693–8703.
20. Lim, H.C., Surovtsev, I.V., Beltran, B.G., Huang, F., Bewersdorf, J., and Jacobs-Wagner, C. (2014). Evidence for a DNA-relay mechanism in ParABS-mediated chromosome segregation. eLife *3*, e02758.
21. Hu, L., Vecchiarelli, A.G., Mizuuchi, K., Neuman, K.C., and Liu, J. (2017). Brownian ratchet mechanisms of ParA-mediated partitioning. Plasmid *92*, 12–16.
22. Bigot, S., Sivanathan, V., Possoz, C., Barre, F.-X., and Cornet, F. (2007). FtsK, a literate chromosome segregation machine. Mol. Microbiol. *64*, 1434–1441.
23. Espéli, O., Borne, R., Dupaigne, P., Thiel, A., Gigant, E., Mercier, R., and Boccard, F. (2012). A MatP-divisome interaction coordinates chromosome segregation with cell division in E. coli. EMBO J. *31*, 3198–3211.
24. Ozaki, S., Jenal, U., and Katayama, T. (2020). Novel divisome-associated protein spatially coupling the z-ring with the chromosomal replication terminus in caulobacter crescentus. mBio *11*, e00487-20.
25. Kois-Ostrowska, A., Strzałka, A., Lipietta, N., Tilley, E., Zakrzewska-Czerwińska, J., Herron, P., and Jakimowicz, D. (2016). Unique function of the bacterial chromosome segregation machinery in apically growing Streptomyces - Targeting the chromosome to new hyphal tubes and its anchorage at the tips. PLoS Genet. *12*, e1006488.
26. Szafran, M.J., Jakimowicz, D., and Elliot, M.A. (2020). Compaction and control-the role of chromosome-organizing proteins in Streptomyces. FEMS Microbiol. Rev. *44*, 725–739.
27. Waite, D.W., Chuvochina, M., Pelikan, C., Parks, D.H., Yilmaz, P., Wagner, M., Loy, A., Naganuma, T., Nakai, R., Whitman, W.B., et al. (2020). Proposal to reclassify the proteobacterial classes *Deltaproteobacteria* and *Oligoflexia*, and the phylum *Thermodesulfobacteria* into four phyla

reflecting major functional capabilities. Int. J. Syst. Evol. Microbiol. *70*, 5972–6016.

28. Rotem, O., Pasternak, Z., and Jurkevitch, E. (2014). *Bdellovibrio* and like organisms. In The Prokaryotes—Deltaproteobacteria and Epsilonproteobacteria (Springer), pp. 3–17.
29. Evans, K.J., Lambert, C., and Sockett, R.E. (2007). Predation by Bdellovibrio bacteriovorus HD100 requires type IV pili. J. Bacteriol. *189*, 4850–4859.
30. Abram, D., Castro e Melo, J., and Chou, D. (1974). Penetration of Bdellovibrio bacteriovorus into host cells. J. Bacteriol. *118*, 663–680.
31. Kuru, E., Lambert, C., Rittichier, J., Till, R., Ducret, A., Derouaux, A., Gray, J., Biboy, J., Vollmer, W., VanNieuwenhze, M., et al. (2017). Fluorescent D-amino-acids reveal bi-cellular cell wall modifications important for Bdellovibrio bacteriovorus predation. Nat. Microbiol. *2*, 1648–1657.
32. Herencias, C., Salgado-Briegas, S., Prieto, M.A., and Nogales, J. (2020). Providing new insights on the biphasic lifestyle of the predatory bacterium Bdellovibrio bacteriovorus through genome-scale metabolic modeling. PLoS Comput. Biol. *16*, e1007646.
33. Fenton, A.K., Kanna, M., Woods, R.D., Aizawa, S.-I., and Sockett, R.E. (2010). Shadowing the actions of a predator: backlit fluorescent microscopy reveals synchronous nonbinary septation of predatory Bdellovibrio inside prey and exit through discrete bdelloplast pores. J. Bacteriol. *192*, 6329–6335.
34. Harding, C.J., Huwiler, S.G., Somers, H., Lambert, C., Ray, L.J., Till, R., Taylor, G., Moynihan, P.J., Sockett, R.E., and Lovering, A.L. (2020). A lysozyme with altered substrate specificity facilitates prey cell exit by the periplasmic predator Bdellovibrio bacteriovorus. Nat. Commun. *11*, 4817.
35. Laloux, G. (2020). Shedding Light on the Cell Biology of the Predatory Bacterium *Bdellovibrio bacteriovorus*. Front. Microbiol. *10*, 3136.
36. Rotem, O., Pasternak, Z., Shimoni, E., Belausov, E., Porat, Z., Pietrokovski, S., and Jurkevitch, E. (2015). Cell-cycle progress in obligate predatory bacteria is dependent upon sequential sensing of prey recognition and prey quality cues. Proc. Natl. Acad. Sci. USA *112*, E6028–E6037.
37. Rendulic, S., Jagtap, P., Rosinus, A., Eppinger, M., Baar, C., Lanz, C., Keller, H., Lambert, C., Evans, K.J., Goesmann, A., et al. (2004). A predator unmasked: life cycle of Bdellovibrio bacteriovorus from a genomic perspective. Science *303*, 689–692.
38. Reyes-Lamothe, R., and Sherratt, D.J. (2019). The bacterial cell cycle, chromosome inheritance and cell growth. Nat. Rev. Microbiol. *17*, 467–478.
39. Gray, K.M., and Ruby, E.G. (1989). Unbalanced growth as a normal feature of development of Bdellovibrio bacteriovorus. Arch. Microbiol. *152*, 420–424.
40. Makowski, Ł., Trojanowski, D., Till, R., Lambert, C., Lowry, R., Sockett, R.E., and Zakrzewska-Czerwińska, J. (2019). Dynamics of chromosome replication and its relationship to predatory attack lifestyles in Bdellovibrio bacteriovorus. Appl. Environ. Microbiol. *85*, e00730-19.
41. Nielsen, H.J., Ottesen, J.R., Youngren, B., Austin, S.J., and Hansen, F.G. (2006). The Escherichia coli chromosome is organized with the left and right chromosome arms in separate cell halves. Mol. Microbiol. *62*, 331–338.
42. Stouf, M., Meile, J.-C., and Cornet, F. (2013). FtsK actively segregates sister chromosomes in Escherichia coli. Proc. Natl. Acad. Sci. USA *110*, 11157–11162.
43. Badrinarayanan, A., Le, T.B.K., and Laub, M.T. (2015). Rapid pairing and resegregation of distant homologous loci enables double-strand break repair in bacteria. J. Cell Biol. *210*, 385–400.
44. Tran, N.T., Laub, M.T., and Le, T.B.K. (2017). SMC progressively aligns chromosomal arms in caulobacter crescentus but is antagonized by convergent transcription. Cell Rep. *20*, 2057–2071.
45. Milner, D.S., Till, R., Cadby, I., Lovering, A.L., Basford, S.M., Saxon, E.B., Liddell, S., Williams, L.E., and Sockett, R.E. (2014). Ras GTPase-like protein MglA, a controller of bacterial social-motility in Myxobacteria, has evolved to control bacterial predation by Bdellovibrio. PLoS Genet. *10*, e1004253.
46. Seidler, R.J., and Starr, M.P. (1968). Structure of the flagellum of Bdellovibrio bacteriovorus. J. Bacteriol. *95*, 1952–1955.
47. Jensen, R.B., and Shapiro, L. (1999). The Caulobacter crescentus smc gene is required for cell cycle progression and chromosome segregation. Proc. Natl. Acad. Sci. USA *96*, 10661–10666.
48. Fogel, M.A., and Waldor, M.K. (2005). Distinct segregation dynamics of the two Vibrio cholerae chromosomes. Mol. Microbiol. *55*, 125–136.
49. Borgnia, M.J., Subramaniam, S., and Milne, J.L.S. (2008). Three-dimensional imaging of the highly bent architecture of Bdellovibrio bacteriovorus by using cryo-electron tomography. J. Bacteriol. *190*, 2588–2596.
50. Butan, C., Hartnell, L.M., Fenton, A.K., Bliss, D., Sockett, R.E., Subramaniam, S., and Milne, J.L.S. (2011). Spiral architecture of the nucleoid in Bdellovibrio bacteriovorus. J. Bacteriol. *193*, 1341–1350.
51. Gray, W.T., Govers, S.K., Xiang, Y., Parry, B.R., Campos, M., Kim, S., and Jacobs-Wagner, C. (2019). Nucleoid size scaling and intracellular organization of translation across bacteria. Cell *177*, 1632–1648.e20.
52. Azam, T.A., Hiraga, S., and Ishihama, A. (2000). Two types of localization of the DNA-binding proteins within the Escherichia coli nucleoid. Genes Cells *5*, 613–626.
53. Lewis, P.J., Thaker, S.D., and Errington, J. (2000). Compartmentalization of transcription and translation in Bacillus subtilis. EMBO J. *19*, 710–718.
54. Bakshi, S., Siryaporn, A., Goulian, M., and Weisshaar, J.C. (2012). Superresolution imaging of ribosomes and RNA polymerase in live Escherichia coli cells. Mol. Microbiol. *85*, 21–38.
55. Winkler, J., Seybert, A., König, L., Pruggnaller, S., Haselmann, U., Sourjik, V., Weiss, M., Frangakis, A.S., Mogk, A., and Bukau, B. (2010). Quantitative and spatio-temporal features of protein aggregation in Escherichia coli and consequences on protein quality control and cellular ageing. EMBO J. *29*, 910–923.
56. Govers, S.K., Dutré, P., and Aertsen, A. (2014). In vivo disassembly and reassembly of protein aggregates in Escherichia coli. J. Bacteriol. *196*, 2325–2332.
57. Ebersbach, G., Briegel, A., Jensen, G.J., and Jacobs-Wagner, C. (2008). A self-associating protein critical for chromosome attachment, division, and polar organization in caulobacter. Cell *134*, 956–968.
58. Laloux, G., and Jacobs-Wagner, C. (2013). Spatiotemporal control of PopZ localization through cell cycle-coupled multimerization. J. Cell Biol. *201*, 827–841.
59. Trojanowski, D., Hołówka, J., and Zakrzewska-Czerwińska, J. (2018). Where and when bacterial chromosome replication starts: A single cell perspective. Front. Microbiol. *9*, 2819.
60. Jensen, R.B., Wang, S.C., and Shapiro, L. (2001). A moving DNA replication factory in Caulobacter crescentus. EMBO J. *20*, 4952–4963.
61. Collier, J., and Shapiro, L. (2009). Feedback control of DnaA-mediated replication initiation by replisome-associated HdaA protein in Caulobacter. J. Bacteriol. *191*, 5706–5716.
62. Arias-Cartin, R., Dobihal, G.S., Campos, M., Surovtsev, I.V., Parry, B., and Jacobs-Wagner, C. (2017). Replication fork passage drives asymmetric dynamics of a critical nucleoid-associated protein in Caulobacter. EMBO J. *36*, 301–318.
63. Bates, D., and Kleckner, N. (2005). Chromosome and replisome dynamics in E. coli: loss of sister cohesion triggers global chromosome movement and mediates chromosome segregation. Cell *121*, 899–911.
64. Berkmen, M.B., and Grossman, A.D. (2006). Spatial and temporal organization of the Bacillus subtilis replication cycle. Mol. Microbiol. *62*, 57–71.
65. Vallet-Gely, I., and Boccard, F. (2013). Chromosomal organization and segregation in Pseudomonas aeruginosa. PLoS Genet. *9*, e1003492.
66. van Raaphorst, R., Kjos, M., and Veening, J.-W. (2017). Chromosome segregation drives division site selection in *Streptococcus pneumoniae*. Proc. Natl. Acad. Sci. USA *114*, E5959–E5968.

67. Ruby, E.G., and Rittenberg, S.C. (1983). Differentiation after premature release of intraperiplasmically growing Bdellovibrio bacteriovorus. J. Bacteriol. *154*, 32–40.

68. Fogel, M.A., and Waldor, M.K. (2006). A dynamic, mitotic-like mechanism for bacterial chromosome segregation. Genes Dev. *20*, 3269–3282.

69. Frage, B., Döhlemann, J., Robledo, M., Lucena, D., Sobetzko, P., Graumann, P.L., and Becker, A. (2016). Spatiotemporal choreography of chromosome and megaplasmids in the Sinorhizobium meliloti cell cycle. Mol. Microbiol. *100*, 808–823.

70. Karunker, I., Rotem, O., Dori-Bachash, M., Jurkevitch, E., and Sorek, R. (2013). A global transcriptional switch between the attack and growth forms of Bdellovibrio bacteriovorus. PLoS ONE *8*, e61850.

71. Milner, D.S., Ray, L.J., Saxon, E.B., Lambert, C., Till, R., Fenton, A.K., and Sockett, R.E. (2020). DivIVA Controls Progeny Morphology and Diverse ParA Proteins Regulate Cell Division or Gliding Motility in *Bdellovibrio bacteriovorus*. Front. Microbiol. *11*, 542.

72. Hu, L., Rech, J., Bouet, J.-Y., and Liu, J. (2020). Spatial control over near-critical-point operation ensures fidelity of ParABS-mediated bacterial genome segregation. bioRxiv. https://doi.org/10.1101/2020.04.26.062497.

73. Guilhas, B., Walter, J.-C., Rech, J., David, G., Walliser, N.O., Palmeri, J., Mathieu-Demazière, C., Parmeggiani, A., Bouet, J.-Y., Le Gall, A., and Nollmann, M. (2020). ATP-driven separation of liquid phase condensates in bacteria. Mol. Cell *79*, 293–303.e4.

74. Wang, X., Liu, X., Possoz, C., and Sherratt, D.J. (2006). The two Escherichia coli chromosome arms locate to separate cell halves. Genes Dev. *20*, 1727–1731.

75. Wu, F., Japaridze, A., Zheng, X., Wiktor, J., Kerssemakers, J.W.J., and Dekker, C. (2019). Direct imaging of the circular chromosome in a live bacterium. Nat. Commun. *10*, 2194.

76. Lambert, C., Chang, C.-Y., Capeness, M.J., and Sockett, R.E. (2010). The first bite–profiling the predatosome in the bacterial pathogen Bdellovibrio. PLoS ONE *5*, e8599.

77. Steyert, S.R., and Pineiro, S.A. (2007). Development of a novel genetic system to create markerless deletion mutants of Bdellovibrio bacteriovorus. Appl. Environ. Microbiol. *73*, 4717–4724.

78. Makowski, Ł., Donczew, R., Weigel, C., Zawilak-Pawlik, A., and Zakrzewska-Czerwińska, J. (2016). Initiation of chromosomal replication in predatory bacterium Bdellovibrio bacteriovorus. Front. Microbiol. *7*, 1898.

79. Kono, N., Arakawa, K., and Tomita, M. (2011). Comprehensive prediction of chromosome dimer resolution sites in bacterial genomes. BMC Genomics *12*, 19.

80. Herencias, C., Prieto, M.A., and Martínez, V. (2017). Determination of the Predatory Capability of Bdellovibrio bacteriovorus HD100. BioProtoc. *7*, e2177.

81. Ferullo, D.J., Cooper, D.L., Moore, H.R., and Lovett, S.T. (2009). Cell cycle synchronization of Escherichia coli using the stringent response, with fluorescence labeling assays for DNA content and replication. Methods *48*, 8–13.

82. Schindelin, J., Arganda-Carreras, I., Frise, E., Kaynig, V., Longair, M., Pietzsch, T., Preibisch, S., Rueden, C., Saalfeld, S., Schmid, B., et al. (2012). Fiji: an open-source platform for biological-image analysis. Nat. Methods *9*, 676–682.

83. Denoncin, K., Nicolaes, V., Cho, S.-H., Leverrier, P., and Collet, J.-F. (2013). Protein disulfide bond formation in the periplasm: determination of the in vivo redox state of cysteine residues. Methods Mol. Biol. *966*, 325–336.

84. Paintdakhi, A., Parry, B., Campos, M., Irnov, I., Elf, J., Surovtsev, I., and Jacobs-Wagner, C. (2016). Oufti: an integrated software package for high-accuracy, high-throughput quantitative microscopy analysis. Mol. Microbiol. *99*, 767–777.

85. Sliusarenko, O., Heinritz, J., Emonet, T., and Jacobs-Wagner, C. (2011). High-throughput, subpixel precision analysis of bacterial morphogenesis and intracellular spatio-temporal dynamics. Mol. Microbiol. *80*, 612–627.

86. van Raaphorst, R., Kjos, M., and Veening, J.-W. (2020). BactMAP: An R package for integrating, analyzing and visualizing bacterial microscopy data. Mol. Microbiol. *113*, 297–308.

87. Lord, S.J., Velle, K.B., Mullins, R.D., and Fritz-Laylin, L.K. (2020). SuperPlots: Communicating reproducibility and variability in cell biology. J. Cell Biol. *219*, 94.

STAR★METHODS

KEY RESOURCE TABLE

REAGENT or RESOURCE	SOURCE	IDENTIFIER
Bacterial strains		
See Table S1.	See Tables S1 and S3	N/A
Chemicals, peptides, and recombinant proteins		
Kanamycin	Sigma	#K4000
Gentamycin	Sigma	#G1914
Ampicillin	Sigma	#A9518
Chloramphenicol	Sigma	#C0378
Novobiocin	Sigma	#74675-1G
DAPI Nucleic Acid Stain	Life Technologies	#D1306
SYTOX orange Nucleic Acid Stain	Life Technologies	#S11368
Syto61 Nucleic Acid Stain	Thermo Fisher	#S11343
FM4-64 Membrane Dye	Invitrogen	#T13320
CellBrite™ Fix 488 Membrane Dye	VWR	#30090-T
Click-iT EdU Alexa Fluor Imaging Kit	Invitrogen	#C10337
SYBR Green	Life Technologies	#4309155
Deposited data		
MATLAB codes and BactMAP cell projections workflow	This study	Zenodo: 10.5281/zenodo.4888934
Oligonucleotides		
See Table S4.	This study	N/A
Recombinant DNA		
See Table S2.	This study	N/A
Software and algorithms		
MATLAB	Mathworks	N/A
Oufti	Paintdakhi:2016ex	http://oufti.org/
NIS-Elements Ar	Nikon Instruments Inc.	N/A
Fiji	Schindelin:2012ir	https://imagej.nih.gov/ij/
Antibodies		
Mouse monoclonal anti-GFP	Takara	#632380; RRID:AB_10013427
Goat anti-mouse IgG-peroxidase	Sigma	#DC02L; RRID: AB_437851
Rabbit polyclonal anti-mCherry	Thermo Fisher	#PA5-34974; RRID: AB_2552323
Goat anti-rabbit IgG-peroxidase	Sigma	#A0545; RRID: AB_257896
Other		
Nikon Ti2-E inverted microscope	Nikon Instruments Inc.	N/A
Prime 95B sCMOS camera	Photometrics	N/A
Synergy H1m microplate reader	Biotek	N/A

RESOURCE AVAILABILITY

Lead contact

Further information and requests for resources and reagents should be directed to and will be fulfilled by the lead contact, Géraldine Laloux (geraldine.laloux@uclouvain.be).

Materials availability

Plasmids and strains generated in this study will be shared by the lead contact upon request.

Data and code availability

Data reported in this paper will be shared by the lead contact upon request. All original Matlab codes used in this paper as well as the workflow to plot cell projections with BactMAP have been deposited at Zenodo (10.5281/zenodo.4888934) and are publicly available as of the date of publication. DOI is listed in the Key resources table. Any additional information required to reanalyze the data reported in this paper is available from the lead contact upon request.

EXPERIMENTAL MODEL AND SUBJECT DETAILS

Strains

All strains and plasmids used in this study are listed in Table S1 and constructed as indicated in Tables S2 and S3. Standard molecular cloning methods were used, and DNA assembly was performed using the NEBuilder HiFi mix (New England Biolabs). All oligos used in this study are listed in Table S4. *B. bacteriovorus* strains were generated from the type strain HD100. *E. coli* strains used as prey were generated from MG1655. *E. coli* strains used for mating were generated from S17-λ*pir*. All plasmids were introduced in *B. bacteriovorus* by mating as described below. Scarless allelic replacements into the HD100 chromosome were performed using a strategy based on the two-step recombination with pK18mobsacB-derived suicide vector as in Steyert and Pineiro,[77] screened by PCR and verified by DNA sequencing. For homology, 500 bp upstream and downstream of the loci of interest were used. Protein fusions were confirmed by western blot (Figure S7B) and predation capacity of genetically engineered strains was verified by killing curves (Figure S7A), as described below.

Locus tags of genes used in this study

dnaN corresponds to Bd0002; *dnaX* corresponds to Bd3731; $parB_{Bb}$ corresponds to Bd3905; *romR* corresponds to Bd2761 (old locus tags from the *B. bacteriovorus* HD100 genome annotation, NCBI Accession number NC_005363). The Bd0063-Bd0064 intergenic integration site is located between nucleotides 58.741 and 58.742.

Labeling of *ori* and *ter*

The *B. bacteriovorus* ori_{Bb} (further named *ori*) has been located between the *dnaA* and *dnaN* genes[78] and the ter_{Bb} region (*ter*) was identified by the 28-bp chromosome dimer resolution site *dif,* found between ORFs Bd2036 and Bd2038.[79] The $parS_{PMT1}$ and $parS_{P1}$ sequences were inserted near these loci by allelic replacement (between ORFs Bd3895 and Bd3896, and between ORFs Bd2052 and Bd2053, i.e., ~17 kbp and 12 kbp away from ori_{Bb} and ter_{Bb}, respectively. We chose insertion sites in non-coding regions of ~60 nucleotides between 3′ ends of predicted ORFs to avoid interrupting transcription initiation signals. The insertion sites between Bd3895 and Bd3896 (between 3.767.999 and 3.767.000), and between Bd2052 and Bd2053 (between 1.958.707 and 1.958.708) are referred to as *ori* and *ter,* respectively, for simplicity; the strains in which $parS_{PMT1}$ or $parS_{P1}$ was inserted at those loci are referred to as *ori*::$parS_{PMT1}$ and *ter*::$parS_{P1}$, respectively.

Routine culturing of *B. bacteriovorus* and *E. coli*

E. coli cells were routinely grown in LB medium except when otherwise stated. *B. bacteriovorus* strains were grown in DNB medium (Dilute Nutrient Broth, Becton, Dickinson and Company, supplemented with 2 mM $CaCl_2$ and 3 mM $MgCl_2$ salts) with *E. coli* as prey at 30°C with constant shaking as previously described (lysates).[80] Two-step revival of *B. bacteriovorus* from −80°C stocks was performed as in Herencias et al.[80] except that only DNB medium was used. When appropriate, antibiotic-resistant *E. coli* strains were used as prey for overnight culturing of the corresponding antibiotics-resistant *B. bacteriovorus*. Kanamycin and gentamycin were used at 50 μg/ml and 10 μg/ml, respectively, both in liquid and solid media.

METHOD DETAILS

Plasmid conjugation by mating

Mating was performed between *E. coli* S17-λ*pir* donor strain carrying the plasmid to be conjugated and the *B. bacteriovorus* receiver strain using a protocol modified from Steyert and Pineiro.[77] Briefly, exponentially growing *E. coli* donor strains were harvested and washed twice in DNB medium before resuspension in 1:10 of the initial volume in DNB-salts. This donor suspension was mixed at equal volume with a fresh overnight lysate of a receiver HD100 strain. The mating mix was incubated for minimum 4 h at 30°C shaking before plating on selective medium using the double layer technique. Single plaques were isolated and transconjugants were confirmed by microscopy (when appropriate), PCR and sequencing.

EdU labeling of newly synthesized DNA

Newly synthesized DNA in *E. coli* and *B. bacteriovorus* cultures was labeled using the Click-iT EdU Alexa Fluor Imaging Kit (Invitrogen, Germany) as performed before with other bacteria.[18,81] Briefly, 200 μl of *B. bacteriovorus* cells grown as indicated or *E. coli* cells grown exponentially in M9-glucose medium were incubated with ~12 μM 5-ethynyl-2′-deoxyuridine (EdU) for 5 and 15 minutes, respectively. Cells were fixed with 78% of ice-cold methanol to stop the reaction, washed in PBS (5000 x *g*, 4°C, 5 min), before membrane permeabilization in 100 μl PBS containing 0.5% Triton X-100 at room temperature for 30 minutes. Hereafter, the detergent was washed off twice with PBS. The pellet was resuspended in 40 μl of Click-iT reaction cocktail and incubated at room temperature

covered from light for 30 minutes. The cells were collected, washed, resuspended in 40 μl of PBS, and when required treated with 5 μg/ml DAPI before imaging.

Live-cell imaging

B. bacteriovorus were first grown overnight with the appropriate *E. coli* prey and antibiotics if maintenance of a plasmid was required, then grown on wild-type MG1655 for at least one generation without antibiotic before the start of the imaging experiment. For snapshots of fresh AP *B. bacteriovorus*, cells were then spotted on 1.2% agarose pads prepared in DNB-salt media. For snapshots of *E. coli* strains, overnight cultures were diluted at least 1:500 and grown to exponential phase before being spotted on 1.2% agarose pads prepared in PBS or M9-salts buffer (supplemented with 0.2% glucose, 0.2% casamino acids and 1μg/ml thiamine, 2 mM $MgSO_4$ and 0.1mM $CaCl_2$). For time-lapse or time-course imaging of synchronous predation cycles, MG1655 *E. coli* cells were grown in 2TYE medium to exponential phase (OD_{600} = 0.4-0.6), harvested at 2600 x g at RT for 5 minutes, washed twice and resuspended in DNB medium. Then, *E. coli* and *B. bacteriovorus* were mixed with a 1:3 to 1:5 volume ratio to allow most prey cells to be infected simultaneously. We consider the prey-predator mixing step as the time 0 in all our synchronous predation imaging experiments. Cells were either spotted directly on DNB-agarose pads for imaging, or left shaking at 30°C before imaging for the indicated durations. In time-lapse experiments, the same fields of view on the pad were imaged at regular interval times as indicated, with the enclosure temperature set to 28°C or 30°C. In time-course experiments, samples from the predation mixture were taken at regular interval times as indicated and directly spotted on agarose pads for snapshots. For nucleoid staining experiments, cells were incubated for 5 min prior imaging with DAPI (Life Technologies), SYTOX orange (Life Technologies) or Syto61 (Thermo Fisher) at a final concentration of 5 μg/ml, 500 nM and 200 nM, respectively. For flagellum staining, *B. bacteriovorus* AP cells were stained with the FM4-64 stain (Thermo Fisher) at a final concentration of 20 μg/ml and incubated in the dark for 2 min before detection or with CellBrite™ Fix 488 Membrane Dye (VWR) at a final concentration of 10X (from a 1:1000 dilution) and incubated in the dark for 2 min before detection. For treatment with novobiocin, fresh AP *B. bacteriovorus* cells were mixed with prey as explained above, treated or not with 5 μg/ml novobiocin (Sigma) at the indicated times and before being immediately spotted on agarose pads containing 5 μg/ml novobiocin or not, respectively.

Image acquisition

Phase contrast and fluorescence images were acquired on a Nikon Ti2-E fully-motorized inverted epifluorescence microscope (Nikon) equipped with CFI Plan Apochromat λ DM 100x 1.45/0.13 mm Ph3 oil objective (Nikon), a Sola SEII FISH illuminator (Lumencor), a Prime95B camera (Photometrics), a temperature-controlled light-protected enclosure (Okolab), and filter-cubes for DAPI, CFP, mCherry, YFP and GFP (Nikon). Multi-dimensional image acquisition was controlled by the NIS-Ar software (Nikon). Pixel size was 0.11 μm or 0.07 μm when using built-in 1X or 1.5X intermediate magnification, respectively. Identical LED illumination and exposure times were applied when imaging several strains and/or conditions in one experiment and were set to the minimum for time-lapse acquisitions to limit phototoxicity.

Image processing

For figure preparation, images were processed with FIJI[82] keeping contrast and brightness settings identical for all regions of interest in each figure, except when otherwise stated. For Figures 4A, 5C, 6A, S5A, and S5B denoising (Denoise.ai, Nikon) was applied on all phase contrast and fluorescence channels to improve the display of time-lapse images acquired with low exposure (which was required to preserve cell viability). For Video S2, Fiji processing ("*Process/Enhance Contrast*") was used to correct for fluorophore bleaching. Figures were assembled and annotated using Adobe Illustrator.

Western blot analysis

Sample preparation for western blot analysis was performed as in Denoncin et al.,[83] starting from 3 mL in the case of cleared *B. bacteriovorus* lysates. Sample were loaded on NuPage Bis-Tris SDS precast polyacrylamide gels and ran at 190 V for 50 minutes in NuPAGE MES SDS running buffer. Western blotting was performed using standard procedures with the following primary antibodies: JL-8 monoclonal antibody (Takara) for GFP variants, YFP and CFP; polyclonal mCherry antibody (product # PA5-34974, Thermo Fisher) for mCherry. Signal from antibody binding was visualized by detecting chemiluminescence from the reaction of horseradish peroxidase with luminol and chemiluminescence was imaged with an Image Quant LAS 500 camera (GE Healthcare). Goat anti-mouse IgG-peroxidase antibody (Sigma) was used as a secondary antibody for JL-8. Goat anti-rabbit IgG-peroxidase antibody (Sigma) was used as a secondary antibody for mCherry. Antibodies were diluted following manufacturer's recommendations. Figures were prepared using ImageJ and assembled and annotated in Adobe Illustrator.

Killing curves

Killing curves assays (Figure S7A) were performed after normalization of the *B. bacteriovorus* inoculum (using the SYBR Green assay described below). Equal amounts of predators from the same fresh cleared lysate were mixed with preys at a final OD_{600} of 0.1, and DNB medium was added to reach 150 μl per well in a transparent 96-well flat bottom plate. Technical triplicates were prepared in separate wells of the same plate in each experiment. The plate was shaken continuously (frequency 567 cpm (3mm)) at 30°C for 24 h in a Synergy H1m microplate reader (Biotek). Optical density measurements at 600 nm were taken every 20 minutes. Decrease of OD_{600} indicates prey lysis, as *B. bacteriovorus* cells do not affect absorbance.

SYBR Green normalization of predator density

For each cleared lysate of *B. bacteriovorus* to analyze, 198 μl/well were transferred into 3 wells of a black 96-well plate with transparent flat bottom (Sigma Aldrich). Then, protected from light, 2 μl of SYBR Green (LifeTechnologies) were added to each replicate to reach a volume of 200 μl per well. Plates without lid were shaken (double orbital, frequency 282 cpm (3 mm)) in a Synergy H1m microplate reader (Biotek), for 15 min at 25°C before one end-point measurement of both OD_{600} and the SYBR Green fluorescence (490 nm excitation, 520 nm emission, gain 55). Based on a standard curve of OD_{600} relative to fluorescence values (obtained from serially diluted *E. coli* suspensions), the contribution of remaining *E. coli* in the lysates to the measured fluorescence was subtracted from the total SYBR Green fluorescence value in each well. The mean of the corrected fluorescence values from the 3 replicates is then used to compare the *B. bacteriovorus* density in different lysates and normalize them accordingly.

QUANTIFICATION AND STATISTICAL ANALYSIS

Cell, nucleoid and spot detection from images

Cell outlines were obtained with subpixel precision from phase contrast images for AP *B. bacteriovorus* cells, uninfected *E. coli* cells or entire bdelloplasts using the automated cellDetection tool in the open-source image segmentation and analysis software Oufti.[84] For analysis of intracellular signal in *B. bacteriovorus* cells within bdelloplasts, predator cell outlines were manually added in Oufti using the same parameters as for AP cells detection. Fluorescent signals were added to cell meshes after background subtraction. Diffraction-limited fluorescent foci and nucleoids (i.e., objects delimited by signals that are beyond the diffraction limit) were detected with subpixel precision from fluorescence images using the spotDetection and objectDetection modules embedded in Oufti, respectively, as described.[84] Features of the detected spots and objects, related to coordinates, morphology and intensity, are added to the corresponding cell in the Oufti cell lists.[84] DAPI was previously demonstrated to be a reliable marker for nucleoid size measurements using this method.[51] For consistency and to allow comparisons, we used the same optimized nucleoid detection parameters on *B. bacteriovorus* and *E. coli* images (Manual background threshold = 0.1; Background subtraction method = 3; Background subtraction threshold = 0.1; Background filter size = 8; Smoothing range (pixels) = 1.5; Magnitude of LOG filter = 0.1; Sigma of PSF = 1.62; Fraction of object in cell = 0.4; Minimum object area = 9). Parameters for spot detection were optimized for each dataset as described,[84] except when analyzing biological replicates or for comparison between strains imaged under identical conditions, in which cases we used the same parameters optimized on the appropriate control set of images.

Quantitative image analysis from cell meshes

Fluorescence-related analysis, nucleoids and spots-related information, as well as other properties of individual cells based on microscopy images were extracted from Oufti data and plotted using custom codes in MATLAB (Mathworks), described below.

Kymographs and demographs

Demographs of relative fluorescence intensity in cells sorted by length were plotted as in Paintdakhi et al.[84] and Sliusarenko et al.[85] When needed, arrays of relative fluorescence were oriented based on the position of the maximal fluorescence intensity of the indicated signal in each cell half. Kymographs were obtained using the built-in kymograph function in Oufti.[84]

Fluorescence profiles

To obtain mean relative fluorescence profiles (*MeanIntProfile.m*), the fluorescence profile of each cell (corresponding to the array of fluorescence intensity provided by the relevant *signal* field in the Oufti cellList) was first normalized by the corresponding *steparea* values (normalization through cellular concentration), then divided by their sum to obtain relative fluorescence values for each cell (to account for potential concentration differences between cells). When needed, arrays of relative fluorescence were oriented based on the position of the maximal fluorescence intensity of the indicated signal in each cell half. Cell length vectors were normalized from 0 to 1 and the corresponding relative fluorescence profiles were interpolated to a fixed dimension vector and concatenated before averaging. Fluorescence intensity profiles along the centerline of individual cells (Figures 4B, S3D, and S4C) were obtained by plotting linescans from segmented lines drawn across each cell in FIJI[82].

Fluorescence spot position and intensity analysis

To obtain spot-to-pole distances (*histSpotsDistPole.m*), the position of single spots along the cell center line was normalized by cell length to obtain relative position values, which were subtracted from 1 if higher than 0.5 in order to obtain relative positions from pole (0) to midcell (0.5). Histograms were then computed and plotted as lines in MATLAB (Mathworks) using built-in functions. Only cells with one spot were kept for this analysis. To obtain the spot/cytosol fluorescence ratio (*RatioSpotFluoVsCellFluo.m*), the relative fluorescence intensity (i.e., total fluorescence divided by area) was calculated for (i) a region of the cell containing the spot, which is defined as the segment where the spot is centered ± 2 segments, and (ii) the cell body, which corresponds to the rest of the cell (i.e., excluding the spot region). The script then computes the ratio of relative fluorescence in the spot versus in the cell body. Fluorescent spots were considered as colocalized in AP cells when the distance between the center of each spot was below a threshold of 200 nm (*colocSpots2signals.m*). Colocalization was evaluated manually for cells inside bdelloplasts.

Nucleoid size measurement

We considered the nucleoid area obtained after running the objectDetection module in Oufti[84] as a proxy for nucleoid size, based on Gray et al.,[51] which showed using a similar detection method that nucleoid area measurements are unaffected by variations in DAPI signal intensity. Nucleoid area is provided by the *object.area* field in the Oufti cell lists, and values were collected in MATLAB for all cells with a single nucleoid and converted to μm^2. Nucleoid area distributions were plotted in MATLAB except violin plots in Figure 2D, which were plotted on R.

Cell Projections using BactMAP

The development version of BactMAP[86] (https://github.com/vrrenske/BactMAP) was used to generate cell projections (Figure S3B). The function orientCells() was written to orient cells by shape and subsequently by their fluorescent focus; cells without focus or with more than one focus were removed from the analysis. After this, the BactMAP function plotOverlay() was used to group cells by cell length into four equally-sized groups and plot the cell shape, DAPI shape and fluorescent spot localization of each cell, faceted by size group.

Killing curve analysis

Features of the curves were extracted by fitting the data to an adaptation of the generalized sigmoid curve (Equation 1) using an R workflow based on a differential evolution algorithm. Briefly, a first rough fit is done using all the data to find an approximation of the sigmoid midpoint *s*. *s* is then used to estimate the sigmoid part of the data on which a second, more accurate fit is performed. Data were plotted using R programming language.

$$P(t) = p_{min} + \frac{p_{max} - p_{min}}{1 + e^{4r_{max}(t-s)/p_{min}-p_{max}}} \quad \text{(Equation 1)}$$

Statistical analyses

The sample sizes and number of repeats are included in the figure legends. Means, standard deviations and coefficients of variation (CV) were calculated in MATLAB (Mathworks) or Microsoft Excel. SuperPlots were generated in Microsoft Excel as described.[87]